

This work was written as part of one of the author's official duties as an Employee of the United States Government and is therefore a work of the United States Government. In accordance with 17 U.S.C. 105, no copyright protection is available for such works under U.S. Law.

Public Domain Mark 1.0

<https://creativecommons.org/publicdomain/mark/1.0/>

Access to this work was provided by the University of Maryland, Baltimore County (UMBC) ScholarWorks@UMBC digital repository on the Maryland Shared Open Access (MD-SOAR) platform.

Please provide feedback

Please support the ScholarWorks@UMBC repository by emailing scholarworks-group@umbc.edu and telling us what having access to this work means to you and why it's important to you. Thank you.

A pure marine aerosol model, for use in remote sensing applications

A. M. Sayer,^{1,2} A. Smirnov,^{2,3} N. C. Hsu,² and B. N. Holben²

Received 5 August 2011; revised 29 November 2011; accepted 30 December 2011; published 15 March 2012.

[1] Retrievals of aerosol optical depth (AOD) and related parameters from satellite measurements typically involve prescribed models of aerosol size and composition, and are therefore dependent on how well these models are able to represent the radiative behavior of real aerosols. This study uses aerosol volume size distributions retrieved from Sun-photometer measurements at 11 Aerosol Robotic Network (AERONET) island sites, spread throughout the world's oceans, as a basis to define such a model for pure (unpolluted) maritime aerosol. Volume size distributions are observed to be bimodal and approximately lognormal, although the coarse mode is skewed with a long tail on the low-radius end. The relationship of AOD and size distribution parameters to meteorological conditions is also examined. As wind speed increases, so do coarse-mode volume and radius. The AOD and Ångström exponent show linear relationships with wind speed, although with considerable scatter. Links between aerosol properties and near-surface relative humidity, columnar water vapor, and sea surface temperature are also explored. A recommended bimodal maritime model, which is able to reconstruct the AERONET AOD with accuracy of order 0.01–0.02, is presented for use in aerosol remote sensing applications. This accuracy holds at most sites and for wavelengths between 340 nm and 1020 nm. Calculated lidar ratios are also provided, and are in the range of other studies, although differ more strongly from those currently used in Cloud-Aerosol Lidar with Orthogonal Polarization (CALIOP) processing.

Citation: Sayer, A. M., A. Smirnov, N. C. Hsu, and B. N. Holben (2012), A pure marine aerosol model, for use in remote sensing applications, *J. Geophys. Res.*, 117, D05213, doi:10.1029/2011JD016689.

1. Introduction

[2] The size distribution and spectral complex refractive index of aerosols are needed to compute properties such as their scattering phase function, single scatter albedo, and extinction coefficient, which are in turn used to calculate quantities such as total aerosol optical depth (AOD) from column abundance. In general, the information content of measurements from current satellite radiometers is insufficient to unambiguously retrieve all these parameters, particularly when the (spectral and directional) behavior of surface reflectance is unknown [Hasekamp and Landgraf, 2007]. For this reason, aerosol retrieval algorithms employed by most of these sensors are required to make assumptions about aerosol microphysical properties, and rely on a set of predefined aerosol models or components. The assumptions in these aerosol retrieval algorithms contribute to differences in retrieved AOD, even in the idealized case of a black (non-reflecting) surface [Kokhanovsky *et al.*, 2010].

The Polarization and Directionality of the Earth's Reflectance (POLDER) sensor is much less restricted, as its measurement capabilities provide an increased information content as compared to most current sensors [Dubovik *et al.*, 2011; Hasekamp *et al.*, 2011].

[3] For other sensors, it is therefore of high importance that the models used are representative of real aerosol properties. The purpose of this study is to develop such a model for clean maritime aerosol, using Sun-photometer data from the Aerosol Robotic Network (AERONET) [Holben *et al.*, 1998]. A companion paper [Sayer *et al.*, 2012] describes the application of this model to aerosol retrievals from Sea-viewing Wide Field-of-view Sensor (SeaWiFS) measurements.

[4] The AOD over the open ocean is typically low (<0.1 in the midvisible [e.g., Smirnov *et al.*, 2009, 2011]). As such, a small absolute bias in a satellite AOD retrieval can translate into a large relative bias. As the Earth's oceans cover approximately two thirds of its surface, and natural marine aerosol is the primary source of cloud condensation nuclei in the remote marine atmosphere, accurate knowledge of the atmospheric aerosol burden is needed for climate modeling studies [e.g., Forster *et al.*, 2007]. Further, by understanding the contribution from pure marine aerosol, the contribution from other aerosol types (such as mineral dust or biomass

¹Goddard Earth Sciences Technology and Research, Universities Space Research Association, Greenbelt, Maryland, USA.

²NASA Goddard Space Flight Center, Greenbelt, Maryland, USA.

³Sigma Space Corporation, Lanham, Maryland, USA.

burning) in conditions of mixed aerosol can be better characterized.

[5] The optical properties of marine aerosol can be determined from ground-based and aircraft in-situ measurements, or theoretical considerations, as well as remote sensing. A review of some of these is presented by *Smirnov et al.* [2002]. In particular, the models of *Shettle and Fenn* [1979] (from aircraft measurements) and *Gathman* [1983] (coastal towers, and ships) have been used widely. However, observational data sets are typically limited in time and space, and differences between the types of instrumentation used in these campaigns contribute to significant differences between the results [*Reid et al.*, 2006]. Advantages of AERONET data therefore include the opportunity to analyze a longer time series, with a wide global distribution, and consistency between different measurement sites. Such studies are also often coastal, such that there may be a non-maritime component to the aerosol. While still a factor for AERONET data, this can be minimized through choice of remote sites, and careful filtering of data. A previous AERONET-based analysis was performed by *Smirnov et al.* [2003a], although at that time the available data record was significantly shorter.

[6] The aerosol number size distribution $dN(r)/d\ln(r)$ describes the number of aerosol particles with radius in the infinitesimal size range $r \pm d\ln(r)$. The distribution is also sometimes defined as $dN(r)/dr$, and these two distributions are easily related by

$$\frac{dN(r)}{dr} = \frac{d\ln(r)}{dr} \frac{dN(r)}{d\ln(r)} = \frac{1}{r} \frac{dN(r)}{d\ln(r)}. \quad (1)$$

[7] The volume size distribution, calculable for spherical aerosol particles as

$$\frac{dV(r)}{d\ln(r)} = \frac{4\pi r^3}{3} \frac{dN(r)}{d\ln(r)}, \quad (2)$$

describing the aerosol particle volume over the same infinitesimal radius range, is also frequently used. The AERONET products are defined in terms of the columnar volume size distribution and so this convention is adopted in the analysis here. The total aerosol columnar particle number (C_n) and volume (C_v) are obtained by integrating these distributions over all $\ln(r)$.

[8] Frequently-used metrics to characterize aerosol size distributions include the logarithmic volume mean radius (r_v) as a measure of the size of the aerosol particles, where

$$\ln(r_v) = \frac{\int_{-\infty}^{\infty} \ln(r) \frac{dV(r)}{d\ln(r)} d\ln(r)}{\int_{-\infty}^{\infty} \frac{dV(r)}{d\ln(r)} d\ln(r)}, \quad (3)$$

and the geometric standard deviation (or spread) of the distribution (σ) as a measure of the dispersion:

$$\sigma = \sqrt{\frac{\int_{-\infty}^{\infty} (\ln(r) - \ln(r_v))^2 \frac{dV(r)}{d\ln(r)} d\ln(r)}{\int_{-\infty}^{\infty} \frac{dV(r)}{d\ln(r)} d\ln(r)}}. \quad (4)$$

[9] The mean radius of the number distribution r_n is defined analogously to equation (3), using $dN(r)/d\ln(r)$ in place of $dV(r)/d\ln(r)$. A third useful quantity is the effective radius (r_{eff}), the ratio of the third to second moments of the number size distribution:

$$r_{\text{eff}} = \frac{\int_{-\infty}^{\infty} r^3 \frac{dN(r)}{d\ln(r)} d\ln(r)}{\int_{-\infty}^{\infty} r^2 \frac{dN(r)}{d\ln(r)} d\ln(r)}. \quad (5)$$

[10] The effective radius is more closely related to aerosol extinction than the number mean radius. This is because scattering depends on aerosol cross-sectional area, and distributions with similar effective radii (and effective variances, although this quantity is less frequently used in aerosol studies) typically have similar scattering properties, even if the precise mean radii and spreads differ [*Hansen and Travis*, 1974; *Mishchenko et al.*, 1997].

[11] Aerosol size distributions are commonly represented as a combination of lognormally-distributed components, and the number size distribution is defined as a summation over these (n_c) components by

$$\frac{dN(r)}{d\ln(r)} = \sum_{i=1}^{n_c} \frac{C_{n,i}}{\sqrt{2\pi}\sigma_i} e^{-\frac{1}{2}\left(\frac{\ln(r) - \ln(r_{n,i})}{\sigma_i}\right)^2}, \quad (6)$$

and the modal radius for each component is also its median and geometric mean. The equivalent distribution for aerosol volume is arrived at by substituting r_n with r_v , and C_n with C_v . The advantages of lognormal distributions include that their statistical properties are well-known, and many available radiative transfer codes are able to take as input lognormal distribution parameters. For individual lognormal components, the conversion between the volume and number distribution parameters is presented in Appendix A. Note that the spread σ remains the same for both number and volume distributions. *Hinds* [1999] presents some general results for moments of lognormal distributions, including that

$$r_{\text{eff}} = r_n e^{2.5\sigma^2} = r_v e^{-0.5\sigma^2}. \quad (7)$$

[12] Section 2 describes the AERONET data used, and properties of average size distributions. Section 3 examines the effect of meteorology on the size distribution. Next, section 4 combines the size information with various refractive indices to define an average aerosol model which is best able to replicate the observed AERONET AODs. Following the definition of this model, section 5 tests the predictive power of the relationship observed between wind speed and aerosol volume on ship-borne AOD measurements, and section 6 presents calculated lidar ratios. Finally, section 7 summarizes the results of the study.

2. AERONET Sites and Size Distribution Data

2.1. Sites and Data Selection Criteria

[13] AERONET data from sites listed in Table 1, and shown in Figure 1, are used here to investigate the characteristics of maritime aerosol. These sites have been chosen due to

Table 1. Locations of the AERONET Sites Used in This Work, as Well as the Number and Proportion of AERONET Inversions Passing the Criteria for Clean Maritime Conditions, as Described in the Text

Site Name	Latitude (deg)	Longitude (deg)	Elevation Above Sea Level (m)	Number of Maritime	Proportion of Maritime
Lanai	20.7350	−156.922	20	1113	0.79
Bermuda	32.3700	−64.6960	10	116	0.49
Kaashidhoo	4.96500	73.4660	0	50	0.20
Midway Island	28.2100	−177.378	20	484	0.86
Ascension Island	−7.97600	−14.4150	30	341	0.61
Tahiti	−17.5770	−149.606	98	375	0.82
Amsterdam Island	−37.8100	77.5730	30	32	0.68
Crozet Island	−46.4350	51.8500	221	8	0.47
Guam	13.4310	144.801	62	74	0.82
Nauru	−0.521000	166.916	7	101	0.91
Graciosa	39.0910	−28.0300	15	57	0.66

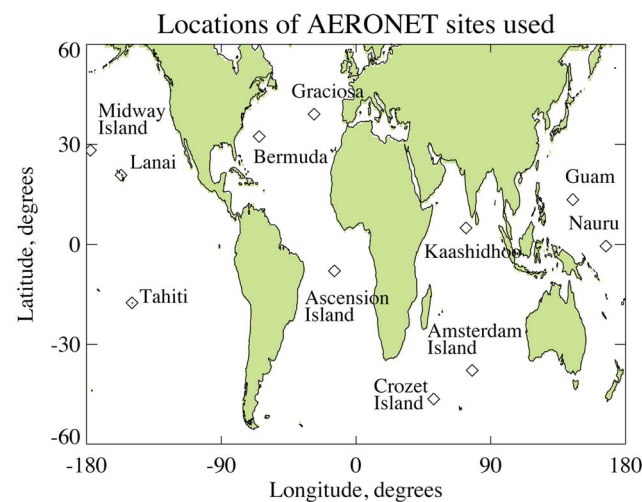
their general remoteness from local sources, in an attempt to exclude the influence of non-maritime aerosols, and span a variety of oceans. The stability and pointing accuracy required to perform the almucantar scans used to retrieve the size distribution means that this technique is impractical aboard moving platforms such as ships, and so island sites represent the closest to open-ocean conditions which can be obtained. Lanai, Bermuda, and Kaashidhoo were previously studied by *Smirnov et al.* [2003a]. A similar study, also examining the effect of wind speed on aerosol properties, was performed for Midway Island by *Smirnov et al.* [2003b]. *Ahmad et al.* [2010] also used AERONET inversions to inform aerosol models for satellite retrievals. The main development of this study over previous work is the improved data record, in terms of an increased number of observations over a larger number of locations, and taking advantage of more recent AERONET algorithm improvements [*Holben et al.*, 2006]. Additionally, some meteorological aspects, and refractive index, are examined in more detail.

[14] For all sites, only version 2 level 2.0 (cloud-screened and quality-assured [*Smirnov et al.*, 2000a; *Holben et al.*, 2006]) data are used. Only retrievals from 1999 onwards are considered, since the newer Sun photometers deployed since then enable a higher data quality. Despite small data records and/or possible influences from other aerosol types, Amsterdam Island, Ascension Island, Crozet Island, Graciosa, and Kaashidhoo are included in the analysis as the most suitable (or only) sites in their respective regions. Kaashidhoo samples air masses transported from the Indian subcontinent, south-east Asia, the Arabian Sea, and the Southern Indian Ocean [*Lobert and Harris*, 2002], while Ascension Island can be affected by transported African biomass burning emissions [*Galanter et al.*, 2000]. Crozet Island has a small data record, due primarily to frequent cloud cover. It also has the highest elevation above sea level (221 m), although this is still within the marine boundary layer. It is included nonetheless as, unlike the majority of other sites, it occupies a cool-sea and high-wind environment.

[15] The AERONET inversion algorithm used to retrieve the aerosol size distribution (in 22 logarithmically-spaced size bins) and refractive index from Sun-photometer measurements is described by *Dubovik and King* [2000] and *Dubovik et al.* [2006]. It takes as input diffuse-sky radiances at 440, 675, 870, and 1020 nm in the solar almucantar, as well as AOD and water vapor from direct-Sun measurements

averaged for 16 minutes before and after the almucantar scan. In this study the AERONET inversions are filtered to select only those retrievals which likely correspond to clean maritime aerosol. Here, τ_λ denotes the AOD at wavelength λ (in nm), and $\alpha = -d\ln(\tau)/d\ln(\lambda)$ the Ångström parameter [*Ångström*, 1929], which describes the spectral variability of τ . The constraints used are that $\tau_{500} \leq 0.2$ (where, if not available directly, τ_{500} is estimated from the nearest available AERONET wavelength and α), and that $0.1 \leq \alpha \leq 1$. In the AERONET record a least-squares fit of all AODs within the 440 nm–870 nm spectral range is used to calculate α to reduce the impact of noise; otherwise, at low optical depths the uncertainty on direct-Sun τ (of order 0.01 [*Holben et al.*, 1998; *Eck et al.*, 1999]) can propagate into significant uncertainties on α (see examples given by *Wagner and Silva* [2008]). All references to α in this study indicate the least-squares fit across this spectral range.

[16] These constraints eliminate cases where there is likely residual cirrus contamination or some non-maritime component (local or transported) to the aerosol loading. The rationale is that urban pollutants and biomass burning are typically fine aerosol particles with large positive α ; desert dust and cirrus clouds have small or negative α ; and the

**Figure 1.** Locations of AERONET sites used in this work.

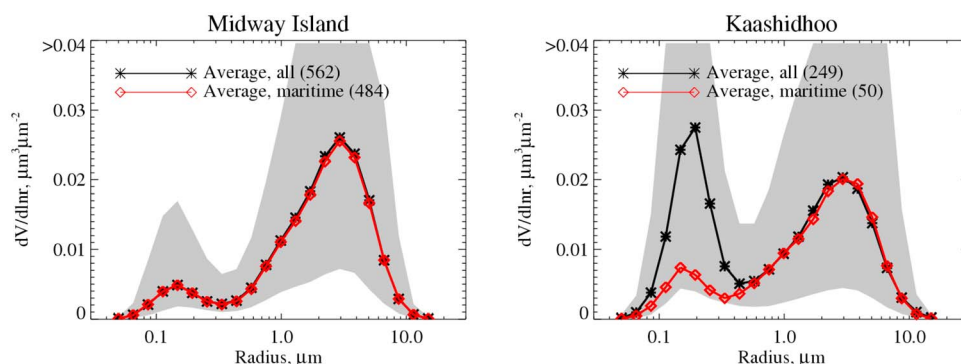


Figure 2. Size-bin-median retrieved aerosol volume size distributions at (left) Midway Island and (right) Kaashidhoo, calculated from all retrieved size distributions (black), and only those distributions meeting the maritime criteria described in the text (red). The shaded region indicates the 5th to 95th percentiles of $dV(r)/d\ln(r)$ encountered in each size bin.

background maritime AOD is typically low [Eck *et al.*, 1999; Kaufman *et al.*, 2001; Dubovik *et al.*, 2002; Knobelspiesse *et al.*, 2004; Smirnov *et al.*, 2009, 2011]. Smirnov *et al.* [2003a] used $\tau_{500} \leq 0.15$ and $\alpha \leq 1$; in this work, the constraints were altered based on manual inspection of size distributions, which revealed that cases where $0.15 \leq \tau_{500} \leq 0.2$ generally still appeared maritime in character (and increased the data volume by approximately 10%), while the lower bound on α removed a small number of distributions which appeared suspect. However, if the thresholds used by Smirnov *et al.* [2003a] are retained, results are numerically very similar. The remaining retrieved size distributions are classified as ‘pure maritime’, and the number of such distributions, as well as the proportion of all distributions meeting these criteria, are given in Table 1.

[17] Midway Island has, of the well-sampled sites, the highest proportion (86%) of retrievals meeting the maritime criteria, and Kaashidhoo the lowest (20%). For these two sites, the average size distributions for all retrievals, and all retrievals designated pure maritime (calculated from the median $dV(r)/d\ln(r)$ in each size bin), are shown in Figure 2. The difference is minimal at Midway Island. At Kaashidhoo, the coarse mode is not significantly different between the two cases. However, the ‘all data’ average shows a significantly stronger fine mode contribution (with a peak around $0.2 \mu\text{m}$), caused by transported continental aerosol particles.

[18] It should be emphasized that these size distributions still represent a retrieval of aerosol properties, rather than direct measurement. Due to the selection of low-AOD cases, AERONET-retrieved refractive indices are not reliable in these situations [Dubovik *et al.*, 2000] and so are not considered. Nevertheless, AERONET offers a much greater sensitivity to aerosol parameters than current satellite instruments, and provides the most comprehensive ground-based data set available, in terms of spatial and temporal coverage, data quality, and consistency of calibration and processing. Additionally, the large sample size, use of medians (discussed later) to decrease sensitivity to outliers (from retrieval error or residual non-marine conditions), and fact that the inversions used pass the AERONET quality control criteria to be raised to level 2 [Holben *et al.*, 2006], mean that the size distributions considered should be suitable for quantitative analysis.

2.2. Properties of Average Size Distributions

[19] For each of the 22 size bins, the median volume density from those inversions meeting the pure maritime criteria has been extracted to define an average size distribution for each site. This is what is meant by the term ‘median’ or ‘average’ distribution through this work (i.e., median calculated for each individual size bin, rather than the median total aerosol volume). If means are used instead then the results are insignificantly affected at most sites (although the total aerosol volume typically increases, as most of the outliers are of higher-than-average volume). Throughout this work, if a median is taken of a set containing an even number of values then the numerically larger is taken; this choice has a negligible impact on the results.

[20] The averaged distributions are shown in Figure 3. The sites all show a similar bimodal volume distribution, with a fine mode peaking at $0.1\text{--}0.2 \mu\text{m}$ and a coarse mode peaking near $3 \mu\text{m}$. Visually it resembles a bimodal lognormal distribution, although the coarse mode is persistently skewed,

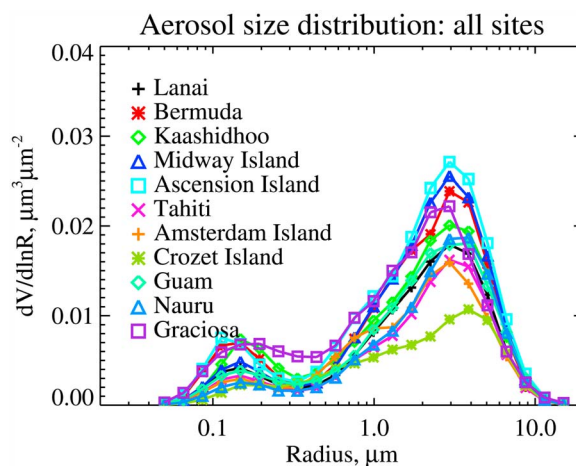


Figure 3. Size-bin-median aerosol volume size distributions for the AERONET sites in Table 1, for measurements corresponding to maritime-type size distributions as described in the text.

Table 2. Size Distribution Parameters for Each Site^a

Site Name	$C_{v,f} (\mu\text{m}^3 \mu\text{m}^{-2})$	$C_{v,c} (\mu\text{m}^3 \mu\text{m}^{-2})$	$r_{v,f} (\mu\text{m})$	$r_{v,c} (\mu\text{m})$	σ_f	σ_c	$r_{\text{eff},f} (\mu\text{m})$	$r_{\text{eff},c} (\mu\text{m})$
<i>AERONET Average Parameters</i>								
Lanai	0.0050 (0.0030)	0.032 (0.013)	0.169 (0.019)	2.39 (0.25)	0.48 (0.04)	0.67 (0.04)	0.151 (0.018)	1.88 (0.19)
Bermuda	0.0080 (0.0044)	0.041 (0.024)	0.159 (0.024)	2.36 (0.51)	0.46 (0.04)	0.65 (0.05)	0.144 (0.021)	1.85 (0.40)
Kaashidhoo	0.0080 (0.0030)	0.037 (0.024)	0.182 (0.013)	2.35 (0.47)	0.45 (0.04)	0.71 (0.06)	0.164 (0.013)	1.76 (0.30)
Midway Island	0.0060 (0.0030)	0.044 (0.024)	0.167 (0.021)	2.41 (0.34)	0.47 (0.04)	0.66 (0.04)	0.149 (0.016)	1.91 (0.26)
Ascension Island	0.0090 (0.0044)	0.049 (0.019)	0.156 (0.015)	2.36 (0.32)	0.48 (0.05)	0.69 (0.03)	0.140 (0.012)	1.84 (0.21)
Tahiti	0.0040 (0.0015)	0.028 (0.013)	0.171 (0.021)	2.43 (0.33)	0.48 (0.03)	0.69 (0.03)	0.153 (0.019)	1.88 (0.23)
Amsterdam Island	0.0050 (0.0030)	0.028 (0.021)	0.183 (0.034)	2.30 (0.30)	0.52 (0.04)	0.70 (0.04)	0.157 (0.027)	1.78 (0.26)
Crozet Island	0.0030 (0.0030)	0.019 (0.022)	0.251 (0.065)	2.17 (0.31)	0.54 (0.10)	0.72 (0.08)	0.220 (0.064)	1.73 (0.16)
Guam	0.0060 (0.0030)	0.035 (0.019)	0.177 (0.031)	2.45 (0.29)	0.49 (0.03)	0.69 (0.03)	0.156 (0.028)	1.91 (0.19)
Nauru	0.0040 (0.0015)	0.031 (0.018)	0.181 (0.031)	2.55 (0.36)	0.49 (0.04)	0.67 (0.04)	0.160 (0.022)	2.00 (0.29)
Graciosa	0.011 (0.0030)	0.042 (0.019)	0.183 (0.019)	2.21 (0.53)	0.50 (0.06)	0.68 (0.07)	0.159 (0.015)	1.69 (0.35)
Mean	0.0063	0.035	0.180	2.36	0.49	0.69	0.159	1.84
Weighted mean	0.0058	0.036	0.168	2.40	0.48	0.68	0.150	1.88
<i>Bimodal Fit to Median Distribution</i>								
Lanai	0.0051 (0.0004)	0.031 (0.002)	0.156 (0.007)	2.55 (0.11)	0.50 (0.05)	0.72 (0.04)	0.138 (0.006)	1.97 (0.08)
Bermuda	0.0081 (0.0006)	0.041 (0.002)	0.145 (0.005)	2.54 (0.12)	0.46 (0.04)	0.73 (0.05)	0.130 (0.005)	1.95 (0.09)
Kaashidhoo	0.0078 (0.0005)	0.037 (0.002)	0.170 (0.005)	2.56 (0.13)	0.44 (0.03)	0.76 (0.05)	0.154 (0.005)	1.93 (0.10)
Midway Island	0.0056 (0.0004)	0.043 (0.002)	0.157 (0.006)	2.58 (0.10)	0.49 (0.04)	0.70 (0.04)	0.139 (0.006)	2.02 (0.08)
Ascension Island	0.0082 (0.0008)	0.047 (0.003)	0.139 (0.007)	2.56 (0.13)	0.45 (0.05)	0.73 (0.05)	0.125 (0.007)	1.96 (0.10)
Tahiti	0.0041 (0.0003)	0.027 (0.002)	0.161 (0.007)	2.72 (0.14)	0.51 (0.05)	0.69 (0.05)	0.141 (0.006)	2.14 (0.11)
Amsterdam Island	0.0037 (0.0002)	0.030 (0.002)	0.155 (0.004)	2.29 (0.15)	0.51 (0.03)	0.84 (0.07)	0.136 (0.004)	1.62 (0.10)
Crozet Island	0.0030 (0.0002)	0.022 (0.002)	0.190 (0.006)	2.54 (0.25)	0.49 (0.03)	0.94 (0.10)	0.168 (0.005)	1.62 (0.16)
Guam	0.0054 (0.0004)	0.034 (0.002)	0.170 (0.008)	2.62 (0.10)	0.56 (0.05)	0.74 (0.04)	0.145 (0.007)	1.98 (0.08)
Nauru	0.0035 (0.0003)	0.031 (0.002)	0.174 (0.009)	2.94 (0.14)	0.55 (0.06)	0.67 (0.05)	0.149 (0.007)	2.34 (0.11)
Graciosa	0.013 (0.001)	0.040 (0.002)	0.210 (0.01)	2.20 (0.094)	0.76 (0.08)	0.76 (0.05)	0.158 (0.011)	1.65 (0.07)
Mean	0.0062	0.035	0.166	2.55	0.52	0.75	0.144	1.93
Weighted mean	0.0057	0.035	0.157	2.59	0.50	0.72	0.138	2.00

^aThe upper half of the table shows median size distribution parameters for AERONET aerosol volume size distributions, and figures in parentheses indicate σ_{med} (defined in the text). The lower half shows bimodal lognormal distribution parameters for fits to bin-median AERONET aerosol volume size distributions, and figures in parentheses indicate one standard deviation uncertainty on the fit. Also shown for both cases are the mean values over all sites, and the mean weighted by the number of AERONET retrievals at each site.

with a wider tail on the low-radius end. The broad similarity between sites is an indication of the similar origins of the aerosol in different global oceans. However, the abundance of both modes can vary, with Ascension Island and Midway Island having notably higher coarse-mode volumes than the other sites. Crozet Island has the smallest aerosol volume, perhaps because of the site's elevation; it is also amongst the most skewed of distributions. Graciosa has the largest fine mode, with a broader distribution and larger particles, suggesting some contribution from local sources.

[21] The AERONET level 2.0 inversion product includes estimates of C_v , r_v , and σ_v (as well as r_{eff}) for the fine and coarse modes (hereafter denoted by subscripts f and c respectively). However, these calculations follow from equations (3) and (4), with the separation between fine and coarse modes determined by estimating the inflection point in the retrieved (binned) size distribution, as opposed to from a fit to an assumed distribution shape. The average of these parameters is given in Table 2 for each site. The uncertainties are given as the scaled median absolute deviation (σ_{med}) about the median for each parameter,

$$\sigma_{\text{med}}(x) = \beta(\widetilde{x - \tilde{x}}), \quad (8)$$

where \sim indicates a median quantity and β is a scaling factor. If the underlying distribution is Gaussian, then σ_{med} is equivalent to the standard deviation for $\beta = 1.4826$, which is assumed here. The use of σ_{med} rather than standard deviation here is again to reduce the sensitivity to outliers, and so provide a more representative estimate of the variability of the

aerosol size distribution parameters in clean maritime conditions.

[22] Given the skewedness exhibited in Figure 3, the averages of the size distribution parameters provided in the AERONET product are not the same as best-fit lognormal distribution parameters from the averaged size distribution. As a distribution constructed from lognormal components is desired, several approaches to addressing this therefore suggest themselves:

1. Use the AERONET-derived parameters from the upper portion of Table 2 directly as bimodal lognormal distribution parameters, even though the underlying distribution is skewed. This will be referred to as the 'AERONET lognormal' method.

2. Fit the average size distribution to a bimodal lognormal distribution. For this method, bins up to and including the inflection point are used to fit the fine mode, and bins with larger r the coarse mode, with a least-squares equal-weighting method. This will be referred to as the 'fitted lognormal' method. Although the bins adjacent to the inflection point may contain volume from both modes, in practice their inclusion or omission was found to have an insignificant effect on the fits.

3. Fit a trimodal lognormal distribution to the retrieved AERONET size distribution, where the larger two modes will represent the skewed coarse mode of a bimodal volume distribution.

[23] The objective is then to determine which of these methods leads to a distribution whose radiative properties match best those of the (non-lognormal) AERONET

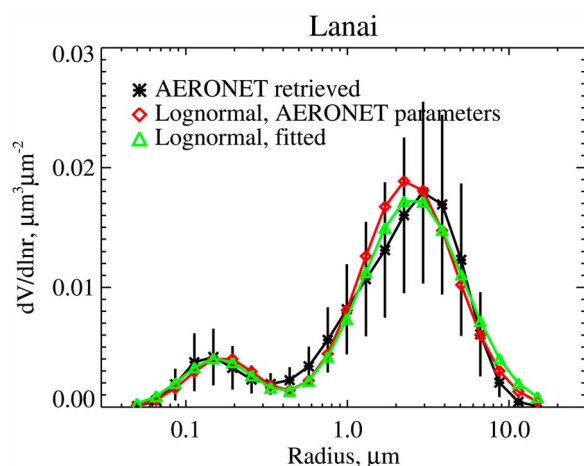


Figure 4. Size-bin-median retrieved aerosol volume size distributions for Lanai (black), and lognormal approximations to it. The distribution constructed from direct use of AERONET parameters is in red, and the best-fit bimodal lognormal distribution in green. Error bars on the retrieved size distribution denote the scaled median absolute deviation, as described in the text.

observations. The preferred method is the simplest one to match within the uncertainties of the data. Trimodal distributions are not investigated here; succeeding sections of this work will show that a bimodal distribution is sufficient and the added complexity of a trimodal distribution is not required for this particular application. In the studies cited throughout this work, bimodal treatments of the aerosol are the more common. An example of the average retrieved distribution, and bimodal lognormal distributions fit to it, is shown for Lanai in Figure 4. Using the AERONET distribution parameters directly for a lognormal distribution results in a larger- r fine mode and smaller- r coarse mode peak than the averaged retrieved AERONET distribution. The fine and coarse mode volumes obtained from both methods are very similar.

[24] The lower portion of Table 2 shows the volume size distribution parameters for each AERONET site for a bimodal lognormal fit, along with uncertainty estimates. For both these and the measured parameters provided by AERONET (Table 2), the parameters are close for most sites, suggesting that an approach to define a global maritime fine-mode and coarse-mode may be successful. Differences between sites may arise from factors such as differences in typical wind speeds or humidity between the sites, or local aerosol particle sources (discussed below).

[25] The largest coarse mode radii are found at Nauru. Henderson *et al.* [2006] report that wind-induced wave-breaking leads to sea salt aerosol production in the coastal surf zone, and formation of downwind cloud trails, at Nauru. It is possible that the larger radii observed by AERONET here arise as a characteristic of this wave-breaking, or the frequent cloud trails mean residual cloud contamination is more likely. Henderson *et al.* [2006] also note that wind at Nauru is predominantly from the east; it is possible that an asymmetric aerosol field could lead to a bias in the AERONET

inversion. Because of this strong surf zone source, results at Nauru may be less representative of the open ocean.

[26] The multisite weighted average fine and coarse effective radii are $0.150\ \mu\text{m}$ and $1.88\ \mu\text{m}$ respectively, when calculated from the AERONET distributions directly (i.e., equation (5)). In comparison, these values are $0.132\ \mu\text{m}$ and $1.70\ \mu\text{m}$ for the ‘AERONET lognormal’ method (i.e., equation (7) applied directly to AERONET distribution parameters), and $0.138\ \mu\text{m}$ and $2.00\ \mu\text{m}$ for the bimodal lognormal fit. The bimodal lognormal fit is closer to for both modes, which provides a first indication that this may more accurately approximate the radiative behavior of the AERONET observations (evaluated in section 4). Overall, these distribution parameters (for both methods) are within the range of other studies (such as summarized by Silva *et al.* [2002] and Smirnov *et al.* [2002, 2003a]). As also noted by Smirnov *et al.* [2003a] and Ahmad *et al.* [2010], the AERONET size distributions are narrower than the older models presented by Shettle and Fenn [1979].

[27] Table 2 shows both mean and number-weighted-mean size distribution parameters. However, from this point the number-weighted values will be used, such that the influence of poorly-sampled sites which more frequently report outlying values (Kaashidhoo, Amsterdam Island, and Crozet Island) is mitigated. The same conclusions broadly hold if the unweighted multi-site mean is used instead, as the weighted and unweighted means are similar.

3. Relationship With Meteorological Parameters

3.1. Data Source

[28] It has long been known that the oceanic aerosol loading is influenced by meteorological factors such as the wind speed or availability of moisture (e.g., Podzimek [1980] gives an earlier review). In this section, the data are therefore examined for these relationships. The National Center for Environmental Prediction (NCEP) reanalysis, available at 1° horizontal resolution output every 6 hours, are used for this purpose [Derber *et al.*, 1991]. Although coarse-resolution, such model output products are nevertheless the only current source of global spatially and temporally complete meteorological data, and so the only recourse if such information is to be used as an input to a global multiyear satellite AOD retrieval scheme.

[29] Wallcraft *et al.* [2009] compared satellite, buoy, and numerical weather prediction (NWP) model (including NCEP) near-surface wind speeds and found each data set exhibited the same spatial patterns, although with regional relative biases. Over most open-ocean regions, including those where most of the sites used here are located, the correlation between NCEP and QuickScat was 0.9 or stronger, and the bias smaller than $0.5\ \text{ms}^{-1}$. The bias and root-mean square difference between NCEP data and buoys were found to be small ($0.15\ \text{ms}^{-1}$ and $0.97\ \text{ms}^{-1}$ respectively). The overall quality of agreement was similar for the different data sets assessed. It is therefore suggested that any of these NWP data sets would provide a reasonable assessment of the near-surface oceanic wind speed near these sites.

[30] Figure 5 compares linearly spatiotemporally interpolated NCEP wind speed and relative humidity near-surface fields with meteorological data recorded at approximately

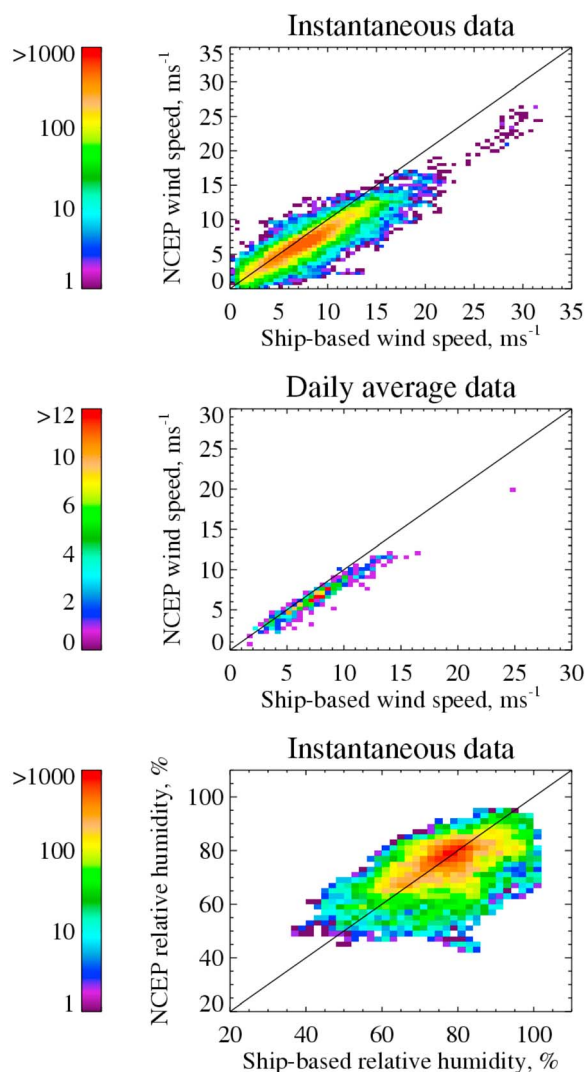


Figure 5. Scatter-density comparison between NCEP and ship-based measurements of wind speed and relative humidity. (top) Instantaneous wind speeds, (middle) daily-averaged wind-speeds, and (bottom) instantaneous relative humidity. Bins without data are shown in white. The bin size is 0.5 ms^{-1} for wind speed and 2% for relative humidity. The 1:1 line is overplotted.

10-minute intervals from twelve cruises of the Research Vessel (RV) Polarstern. These cruises are Atlantic Ocean transects, chosen to cover the latitude range inhabited by the relevant AERONET sites, and sampling a wide range of wind speeds [König-Langlo, 2011]. Overall the correspondence is high, although the coarser spatial and temporal resolution of the NCEP data mean there is a tendency for extrema to be missed. When these instantaneous wind speeds are averaged to daily values, the gradient of the least-squares best fit line forced through zero does not change much (0.84 to 0.85), i.e., the NCEP data tend to underestimate the wind speed. However, the correlation increases from 0.90 to 0.96. For relative humidity, the data are almost unbiased (gradient 0.97) although the correlation coefficient is lower (0.54). These results support the validity of the use

of NCEP data for the analysis of the relationship of aerosol properties with meteorology. However, the differences underscore the fact that analyses of this type are sensitive to not only the quality of the aerosol data, but also the meteorological data. Part of the discrepancy may be due to the altitude difference (10 m for NCEP, as compared to 25 m above sea level for the ship).

[31] Additional AERONET aerosol products provide further insight into the relationship between marine aerosol and the ambient conditions. Firstly, although the AERONET size distribution inversions include temporal averages of direct-Sun AODs (as discussed previously), the full direct-Sun data set is significantly larger. The second avenue is through the spectral deconvolution algorithm (SDA) data product, which provides the partition of AOD at 500 nm into separate contributions from the fine and coarse mode, and is independent of the other AERONET aerosol retrieval algorithms ([O'Neill *et al.*, 2003, 2006] for the current version 4 level 2.0 data set).

[32] Both of these additional products are therefore considered. As before, the restrictions that $\tau_{500} \leq 0.2$, $0.1 \leq \alpha \leq 1$, and data from 1999 onwards, are imposed. Additionally, to decrease the noise, and because of the coarser NCEP resolution, after obtaining the meteorological information for each case, the direct-Sun and SDA products are down-sampled to daily averages for the comparisons with wind speed and relative humidity before these thresholds are applied. This provides between 105 (Graciosa) and 1,171 (Midway Island) dates per site, with typically around 15 measurements contributing to each daily average. This daily averaging is not done for the size distribution inversions, as these are less frequent (many days have multiple direct-Sun measurements but no size distribution inversions). Additionally, the data are not averaged for the water vapor comparisons, as these are part of the AERONET product and so do not require matching with additional NCEP data.

3.2. Dependence on Wind Speed

[33] Previous studies based on both satellite and ground-based data have shown that increased near-surface wind speeds (w_s) are associated with an increase in AOD, due to wind increasing the flux of sea spray (i.e., increased aerosol mass), and water vapor (i.e., aerosol swelling), from the ocean to the marine boundary layer [Zieliński and Zieliński, 2002; Smirnov *et al.*, 2003b; Satheesh *et al.*, 2006; Mulcahy *et al.*, 2008; Sakerin *et al.*, 2008; Glantz *et al.*, 2009; Huang *et al.*, 2010; Lehahn *et al.*, 2010; Adames *et al.*, 2011; Grandey *et al.*, 2011; Kiliyanpilakkil and Meskhidze, 2011]. These are similar to earlier results which directly sampled aerosol particles, rather than remotely-sensed AOD [e.g., Lovett, 1978; Blanchard and Woodcock, 1980; Monahan *et al.*, 1983; Exton *et al.*, 1985; Hoppel *et al.*, 1990]. However, stronger wind speeds mean that the aerosol will be transported downwind of its source more rapidly, and so simple relationships between the two quantities are unlikely to capture all of the variability in aerosol loading, unless meteorological conditions are homogeneous over a large area and time period, and there are no other aerosol sources.

[34] Stronger correlations have been observed using the wind speed averaged over some time before the aerosol measurements were made ('wind speed history'), rather than instantaneous wind speed, as wind changes on timescales shorter than aerosol lifetimes. The strongest correlations are

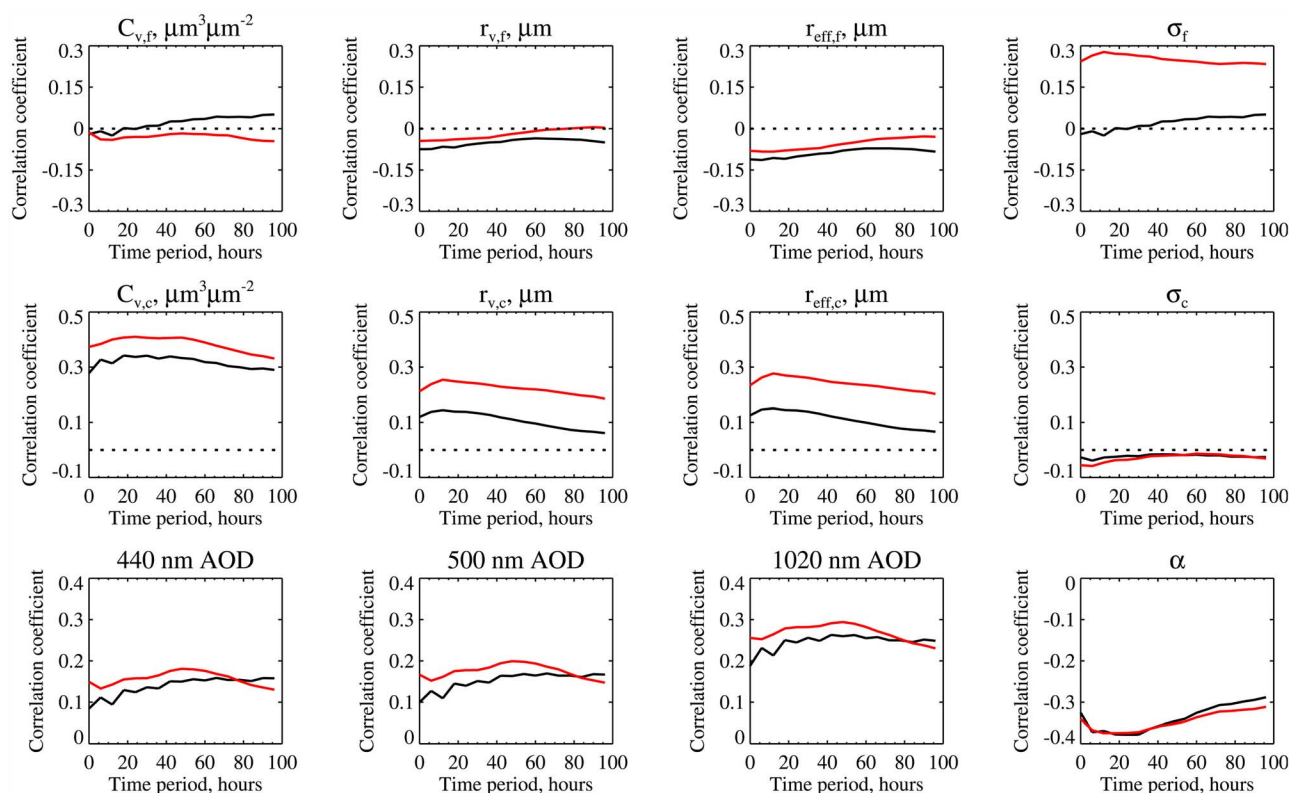


Figure 6. Pearson's linear correlation coefficient between time-averaged wind speed (prior to the AERONET observation time) and AERONET aerosol inversion data. The black lines show correlations for all data points combined. The red lines show the multi-site mean of correlations calculated individually for each site with 100 or more AERONET inversions.

typically found with wind speed averaged for 12–24 hours prior to the AOD measurement [Gathman, 1983; Hoppel *et al.*, 1990; Smirnov *et al.*, 2003b; Lehahn *et al.*, 2010]. Some of these analyses bin data by wind speed, and then fit binned averages; this binning will naturally lead to stronger correlations than fits using all data points, as the variability is somewhat averaged-out, so this should be borne in mind when examining regression statistics from different studies. Mulcahy *et al.* [2008] found, for stable wind conditions, a very strong relationship between bin-average AOD and the approximate square of the wind speed. However, this was based upon measurements at a coastal site, and it is possible that breaking waves on the rocky shore would lead to the production of additional aerosol above what would be observed in open-ocean (i.e., rock-free) conditions, or that there are differences in wind conditions between the coast and nearby ocean [Blanchard and Woodcock, 1980; Henderson *et al.*, 2006]. It is uncertain whether these trends continue for high wind speeds, due to a paucity of data for $ws \approx 10 \text{ ms}^{-1}$ or higher, and the few observations in these conditions have shown either increases, leveling-off, or decreases in aerosol loading [Blanchard and Woodcock, 1980; Exton *et al.*, 1985; Mulcahy *et al.*, 2008; Pant *et al.*, 2008; Grandey *et al.*, 2011; Kiliyanpilakkil and Meskhidze, 2011].

[35] In this analysis, for each AERONET size distribution, NCEP near-surface (10 m) wind speed data points are linearly interpolated in space and time to provide the

'instantaneous' wind speed. The wind speed history is then defined by repeating this procedure backwards in time in 6 hour increments, and averaging the resulting wind speed for up to 96 hours prior to the time of the AERONET retrieval. Pearson's linear correlation coefficient between aerosol parameters and this time-averaged wind speed are shown in Figure 6, separately calculated using all AERONET data together, as well as the multi-site mean correlation from those sites with 100 or more AERONET inversions. The correlations with the size distribution parameters are calculated using those directly reported by AERONET (i.e., those from which the averages in the upper part of Table 2 were computed) rather than those from lognormal fits; similar results are obtained if the lognormal fit results are used instead.

[36] The two methods of showing correlations in Figure 6 give very similar results. Correlations are often slightly stronger when the mean correlation from the well-sampled sites is shown, rather than using all data together. Even if the true response of aerosol to changes in wind speed were the same at each AERONET site, the strengths of correlations might be expected to vary due to factors such as how well the coarse-resolution NCEP data represent the real wind speed; the range of wind speeds observed at a given location (if the response of the aerosol is nonlinear); and the fact that the sites are above sea level, so if a significant proportion of the aerosol response takes place below the site then this may be missed in the AERONET data if the aerosol is not

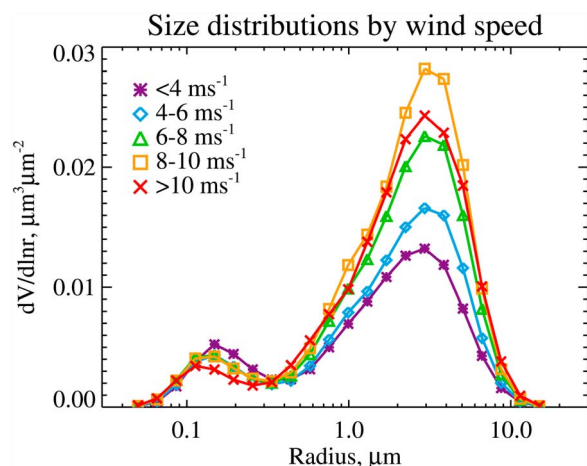


Figure 7. Size-bin-median AERONET aerosol volume size distributions, binned by near-surface wind speed.

vertically well-mixed. *Blanchard and Woodcock* [1980] present a model for the vertical dependence of sea salt concentration, based on wind speed; according to this, the highest number of particles are found at heights of up to 0.2 m above the sea surface, but most of these particles rapidly fall back in. For heights of meters to several hundreds of meters, there is a small decline with height, with an eventual inversion layer of increasing concentration in the range 300 m to 600 m. Non-sea-salt components were not considered. It is therefore likely that altitude and background aerosol contribute to the differences between sites. The issue is complicated by the fact that the results of *Blanchard and Woodcock* [1980] were collected in cloudy conditions, while the AERONET data are clear-sky; *Blanchard and Woodcock* [1980] note that the salt inversion layer may depend on boundary-layer cloudiness.

[37] Positive correlations are found between the wind speed history and aerosol volume, particularly for the coarse mode, consistent with previously-mentioned studies. This manifests in additional positive correlations with AOD, stronger for τ_{1020} than τ_{440} , and a negative correlation with α , all linked to the fact that the fine mode is more optically-active in the visible, and the coarse mode in the near-infrared. There are also positive correlations between r_v and the wind speed history, while the correlation is positive for the fine mode spread but negative for the coarse mode. These correlations are, however, generally weaker than those observed for C_v , τ , and α , which themselves are typically 0.4 or smaller.

[38] Given the observed correlations, the next step is to examine the size of the response of the aerosol size

distribution to wind speed. For this purpose, averaged size distributions (as described previously) have been calculated by binning the AERONET inversions according to the NCEP wind speed rather than by site. Bins have been chosen such that a large number of inversions fall within each, although there were only 61 cases of winds stronger than 10 ms^{-1} , meaning care should be taken when considering results for high winds. Removing the constraints on τ_{500} and α at Lanai and Midway (the most well-sampled sites) does not result in significantly more high-wind points, implying that these imposed constraints are not causing a sampling bias in wind speed. Approximately 85% of inversions were for wind speeds from $4\text{--}10 \text{ ms}^{-1}$. The resulting size distributions are shown in Figure 7. Table 3 details the number in each bin, τ , and α , and shows the expected increase of AOD with wind speed and corresponding decrease of α . The wavelengths shown in Table 3 and later in the analysis are chosen as the shortest and longest in the AERONET record, plus 500 nm as a frequently-used reference wavelength. Size distribution parameters (for both the median of the corresponding AERONET inversion parameters, and log-normal fits to the median of distributions) are given in Table 4. The highest winds have a slightly lower AOD than anticipated by this trend, due to a slight decrease in the aerosol volume, although as mentioned sampling is comparatively poor for this range, and the difference in AOD and aerosol volume between the two highest wind speed bins is within the variability of each bin.

[39] The base AOD for the calmest waters appears to be 0.068 at 440 nm, 0.065 at 500 nm, and 0.035 at 1020 nm. This is similar to background AOD at 870 nm for dust-free period at Barbados of 0.035–0.04 reported by *Smirnov et al.* [2000b]. The results for typical wind speeds also match well the ‘baseline maritime’ AOD at 500 nm of order 0.052–0.071 reported by *Kaufman et al.* [2001], and observations taken on the decks of ships [*Smirnov et al.*, 2011].

[40] It is observed that, as wind speed increases, fine mode properties show mixed trends. The change in $C_{v,f}$ is small, but potentially a decrease as wind speeds increase. The coarse mode exhibits a larger change; $C_{v,c}$ increases strongly with higher winds, consistent with the previously-mentioned studies. The difference between bin averages for the lowest and highest winds is a factor of two. Additionally, $r_{v,c}$ increases, although σ_c varies less strongly. The increase of $r_{\text{eff},c}$ is driven mostly by the changes in $r_{v,c}$.

[41] The difference between $r_{v,c}$ for the two most populated bins ($4\text{--}6 \text{ ms}^{-1}$ and $6\text{--}8 \text{ ms}^{-1}$) is within the variability of distributions in each bin (for the ‘AERONET lognormal’ method) and smaller than the fit uncertainty on each bin (for the ‘lognormal fitted’ method). The same is true for σ_c . They are also smaller than or comparable to the variability or fit

Table 3. Number of Retrievals, AOD at Three Wavelengths, and Ångström Exponent Corresponding to AERONET Aerosol Volume Size Distributions, Binned as a Function of Near-Surface Wind Speed^a

Wind Speed	Number of Retrievals	τ_{440}	τ_{500}	τ_{1020}	α
0–4 ms^{-1}	331	0.068 (0.025)	0.065 (0.023)	0.035 (0.014)	0.75 (0.14)
4–6 ms^{-1}	965	0.065 (0.019)	0.061 (0.017)	0.038 (0.012)	0.61 (0.17)
6–8 ms^{-1}	1051	0.076 (0.024)	0.072 (0.022)	0.051 (0.017)	0.50 (0.18)
8–10 ms^{-1}	291	0.079 (0.024)	0.076 (0.023)	0.057 (0.019)	0.38 (0.16)
10+ ms^{-1}	61	0.075 (0.025)	0.075 (0.025)	0.059 (0.023)	0.36 (0.16)

^aFigures in parentheses indicate σ_{med} .

Table 4. Size Distribution Parameters for Average Distributions Binned as a Function of Near-Surface Wind Speed^a

Wind Speed	$C_{v,f}$ ($\mu\text{m}^3\mu\text{m}^{-2}$)	$C_{v,c}$ ($\mu\text{m}^3\mu\text{m}^{-2}$)	$r_{v,f}$ (μm)	$r_{v,c}$ (μm)	σ_f	σ_c	$r_{\text{eff},f}$ (μm)	$r_{\text{eff},c}$ (μm)
<i>AERONET Average Parameters</i>								
0–4 ms^{-1}	0.0070 (0.003)	0.025 (0.010)	0.174 (0.014)	2.29 (0.25)	0.46 (0.023)	0.68 (0.034)	0.157 (0.012)	1.77 (0.18)
4–6 ms^{-1}	0.0060 (0.002)	0.030 (0.0090)	0.168 (0.014)	2.38 (0.20)	0.47 (0.026)	0.68 (0.028)	0.150 (0.012)	1.87 (0.14)
6–8 ms^{-1}	0.0060 (0.002)	0.040 (0.012)	0.166 (0.014)	2.43 (0.19)	0.48 (0.026)	0.68 (0.026)	0.148 (0.012)	1.91 (0.14)
8–10 ms^{-1}	0.0060 (0.002)	0.050 (0.015)	0.167 (0.014)	2.45 (0.19)	0.50 (0.027)	0.67 (0.030)	0.149 (0.011)	1.92 (0.16)
10+ ms^{-1}	0.0050 (0.002)	0.048 (0.017)	0.166 (0.019)	2.45 (0.29)	0.52 (0.019)	0.69 (0.037)	0.146 (0.016)	1.90 (0.20)
<i>Bimodal Fit to Median Distribution</i>								
0–4 ms^{-1}	0.0061 (0.0004)	0.025 (0.001)	0.167 (0.0052)	2.34 (0.087)	0.48 (0.033)	0.75 (0.038)	0.149 (0.0046)	1.76 (0.065)
4–6 ms^{-1}	0.0052 (0.0004)	0.030 (0.002)	0.156 (0.0066)	2.54 (0.11)	0.49 (0.045)	0.73 (0.045)	0.138 (0.0059)	1.95 (0.087)
6–8 ms^{-1}	0.0055 (0.0005)	0.039 (0.002)	0.152 (0.0078)	2.63 (0.12)	0.51 (0.055)	0.71 (0.045)	0.133 (0.0069)	2.04 (0.091)
8–10 ms^{-1}	0.0055 (0.0005)	0.047 (0.003)	0.154 (0.0087)	2.70 (0.13)	0.53 (0.061)	0.69 (0.046)	0.134 (0.0076)	2.13 (0.099)
10+ ms^{-1}	0.0040 (0.0003)	0.044 (0.002)	0.137 (0.0057)	2.64 (0.11)	0.47 (0.046)	0.73 (0.041)	0.122 (0.0051)	2.02 (0.083)

^aThe upper half of the table shows averaged (median) size distribution parameters for AERONET aerosol volume size distributions, and figures in parentheses indicate σ_{med} (defined in the text). The lower half shows bimodal lognormal distribution parameters for fits to averaged AERONET aerosol volume size distributions, and figures in parentheses indicate one standard deviation uncertainty on the fit.

uncertainty of these parameters at individual sites (Table 2). Additionally, the values of these parameters for the 0–4 ms^{-1} and 8–10 ms^{-1} bins are typically within or close to the variability or fit uncertainty. These are important results as they indicate that the multi-site average $r_{v,c}$ and σ_c may be able to represent coarse-mode aerosol for the majority of encountered wind strengths. This highlights again the underlying similarity of the coarse-mode aerosol at different locations (i.e., aerosol found at different locations with similar wind speeds correspond more closely than aerosol observed at a single location over a range of wind speeds). The results change insignificantly if size distributions are binned by the 24-hour-average, rather than instantaneous, wind speed.

3.2.1. Fits of C_v to Wind Speed

[42] Figure 8 shows least-squares linear regressions between AERONET retrieved fine and coarse mode volumes ($C_{v,f}$ and $C_{v,c}$) to the wind speed (both instantaneous and 24-hour averaged). Data from all sites are shown together, averaged in bins of 0.5 ms^{-1} . Bin medians are used to reduce the effect of outliers on the fit. Several bins at very low and high winds contained small numbers of retrievals, and as these bins lie at the edges of the range they have a strong influence on the linear least-squares fit. For this reason, bins with fewer than 50 size distributions have been excluded from the analysis. However, this means that the

relationship spans only wind speeds from approximately 2–10 ms^{-1} . The fine mode volume is independent of wind speed, while the coarse shows a positive response, consistent with the mechanism of wind-driven emission. For the fine mode, quantization in the AERONET C_v (increments of 0.001) is evident in the fit. Between the quantization and variability within each bin, there is effective no relationship for the fine mode.

[43] The fits were also performed on the raw unbinned data at all sites and on a site-by-site basis (omitted for brevity), although the large amount of scatter and impossibility of AERONET retrieving a negative aerosol volume lead to fits more strongly influenced by outlying points, and not capturing the variability of the bulk of the data well. Exponential fits were attempted in addition to linear, although over the wind speed range considered the differences in the best-fit line were negligible (i.e., any nonlinearity in the true relationship is sufficiently small as to be undetectable at the wind speed range observed). Similar fit coefficients, generally within the uncertainty of the linear fit, were obtained at each site: almost no relationship with wind speed for the fine mode volume, and near-linearity for coarse mode.

[44] These results imply that, if only the wind speed or wind speed history is known, assuming $C_{v,f} \approx 0.0057$ (i.e., the average observed value) and $C_{v,c} \approx 0.018 + 0.0027ws$ or

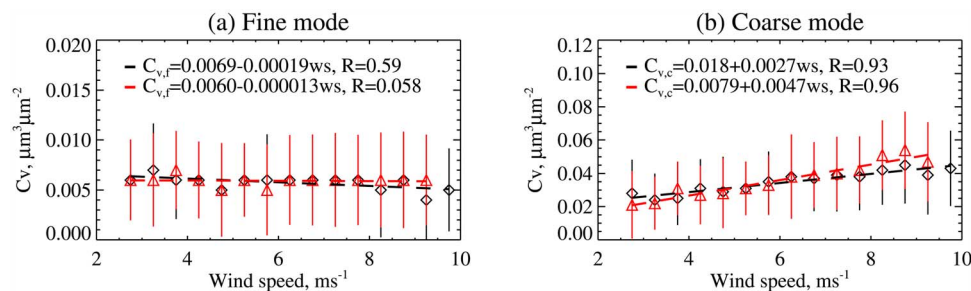


Figure 8. Relationship between wind speed and aerosol volume for (a) fine and (b) coarse modes, binned by wind speed in bins of 0.5 ms^{-1} . Black diamonds show data binned by spatiotemporally interpolated NCEP wind speeds, and red triangles data binned by NCEP wind speed averaged over the 24-hour-period prior to the retrieval. Error bars show the standard deviation on each bin's data. Coefficients of linear fit are given in the plots, and illustrated with dashed lines; R indicates Pearson's linear correlation coefficient. Data are only shown where a bin contains at least 50 data points.

Table 5. Statistics of Linear Regression Between Wind Speed and AOD or α (Daily Averages for Both Data Sets) of the Form τ (or α) = $a + b \times ws$, From Direct-Sun and SDA AERONET Data^a

Site	τ_{440}			τ_{1020}			α			τ_{500}			$\tau_{500,f}$			$\tau_{500,c}$		
	<i>a</i>	<i>b</i>	<i>R</i>	<i>a</i>	<i>b</i>	<i>R</i>	<i>a</i>	<i>b</i>	<i>R</i>	<i>a</i>	<i>b</i>	<i>R</i>	<i>a</i>	<i>b</i>	<i>R</i>	<i>a</i>	<i>b</i>	<i>R</i>
Lanai	0.092	-0.0021	0.13	0.044	0.00058	0.053	0.79	-0.039	0.35	0.084	-0.0015	0.0045	0.042	-0.0021	0.025	0.040	0.00056	-0.030
Bermuda	0.097	0.0028	0.20	0.053	0.0029	0.29	0.82	-0.024	0.31	0.089	0.0025	-0.097	0.046	-0.000021	0.0070	0.042	0.00026	-0.16
Kaashidhoo	0.12	0.0022	0.091	0.070	0.0033	0.18	0.70	-0.036	0.27	0.110	0.0027	-0.17	0.052	0.00013	-0.14	0.056	0.00036	-0.13
Midway Island	0.069	0.0044	0.25	0.033	0.0051	0.37	0.76	-0.039	0.40	0.065	0.0043	0.023	0.034	-0.00017	0.068	0.029	0.0045	-0.00003
Ascension Island	0.090	0.0053	0.13	0.047	0.0039	0.12	0.71	-0.024	0.11	0.080	0.0052	-0.034	0.039	0.00070	-0.084	0.041	0.0045	0.14
Tahiti	0.082	0.00041	0.024	0.029	0.0011	0.058	0.72	-0.021	0.17	0.079	0.00029	-0.15	0.032	-0.00014	0.0062	0.043	0.00057	-0.19
Amsterdam Island	0.057	0.0030	0.30	0.033	0.0032	0.37	0.58	-0.013	0.17	0.053	0.0031	-0.13	0.016	0.0011	-0.11	0.034	0.00020	-0.12
Crozet Island	0.061	0.0015	0.12	0.044	0.0016	0.16	0.55	-0.011	0.13	0.056	0.0017	0.0043	0.021	0.00052	-0.024	0.033	0.0012	0.030
Guam	0.097	0.00007	0.0029	0.051	0.0031	0.16	0.90	-0.074	0.48	0.091	0.00092	-0.15	0.051	-0.00023	-0.056	0.036	0.00034	-0.12
Nauru	0.055	0.0041	0.24	0.028	0.0047	0.23	0.60	-0.039	0.26	0.054	0.0041	-0.050	0.022	0.00055	-0.085	0.030	0.00038	-0.025
Graciosa	0.16	-0.0039	0.26	0.089	-0.0012	0.095	0.73	-0.017	0.18	0.150	-0.0034	0.24	0.078	-0.00029	0.31	0.070	-0.00060	0.046
All sites	0.072	0.0035	0.19	0.034	0.0039	0.26	0.65	-0.022	0.21	0.070	0.0031	0.19	0.031	0.00035	0.042	0.036	0.00029	0.24

^a Also shown is Pearson's Linear correlation coefficient for the fit, *R*. The top section shows results for τ_{440} , τ_{1020} , and α . The bottom section shows results for τ_{500} , for each of total AOD and the contributions from fine and coarse modes. In each section, the final row shows the fits when data from all sites are considered together.

$C_{v,c} \approx 0.0079 + 0.0047ws$ (i.e., the global average best linear relationship for the binned data, dependent on whether instantaneous or 24-hour-averaged wind speed is known) will give a reasonable first-order estimate of the aerosol volume. This is examined further in section 5. Despite this, wind speed alone is likely to be a poor predictor of aerosol volume; the variability within bins on Figure 8 is similar to the range of volumes encompassed by the best-fit line. This highlights the necessity for complexity and consideration of the aerosol life cycle from emission to removal in modeling of the aerosol burden, as is performed by the current generation of global models.

3.2.2. Fits of AOD to Wind Speed

[45] Statistics of linear fits of direct-Sun AOD and α to wind speed (in both cases, from points averaged for each day) are presented in Table 5. There is considerable variety between the sites, both in terms of strength of correlation and the fit parameters, which may in part reflect different local sources. In general, the strongest agreement is found between *ws* and α ; stronger correlations are found with τ_{1020} than τ_{440} . These results can again be explained in terms of an increased coarse-mode presence at higher wind speeds. Due to the high scatter, the uncertainties on these linear fit parameters (not shown) are large. The SDA results are consistent with this: $\tau_{500,f}$ is independent of wind speed and around 0.031, while $\tau_{500,c}$ has a similar magnitude in the absence of wind (0.036) but a positive gradient of $0.0029 \text{ m}^{-1}\text{s}$.

[46] Averaging the data over all sites in bins of 0.5 ms^{-1} , and taking the bin medians, leads to the relationships shown in Figure 9. Again, poorly-sampled bins (fewer than 50 points) are omitted. An approximate linear relationship appears to hold for all cases. As with aerosol volume, the variability within each bin is similar to or larger than the range of the bin-average values, again illustrating that wind speed alone is of limited utility in predicting the marine aerosol burden for an individual case. However, the link between wind and an increased coarse-mode contribution to the AOD is evident.

3.2.3. Joint Analysis With Sea Surface Temperature

[47] Marine (sea spray) aerosol source functions in Earth system models are typically the product of an assumed size distribution with a (wind-speed-dependent) fractional whitecap cover, although there is considerable scatter between different parameterizations [Lewis and Schwartz, 2004; O'Dowd and de Leeuw, 2007]. Jaeglé *et al.* [2011] improved the correspondence between modeled and observed sea salt aerosol burdens by modifying the source function of Gong [2003] with an empirical sea surface temperature (SST)-dependent correction. This dependence has been known for some time and is thought to arise partially due to the changing kinematic viscosity of the sea surface with temperature (determining bubble rising and breaking), and partially because observed whitecap fraction is also linked to SST [Podzimek, 1980; Anguelova and Webster, 2006]. An SST dependence has also been observed in laboratory studies of seawater and analogues [Sellegrí *et al.*, 2006, and references therein].

[48] Due to diurnal changes in SST, aerosol lifetimes on the order of days, and the fact that the AERONET sites are not located at the ocean surface, the observed aerosol in the atmosphere at any given time may not be representative of the aerosol flux from the ocean for the temperature at that given time, and there is no direct match possible between SST and the AERONET inversions. For these reasons, the

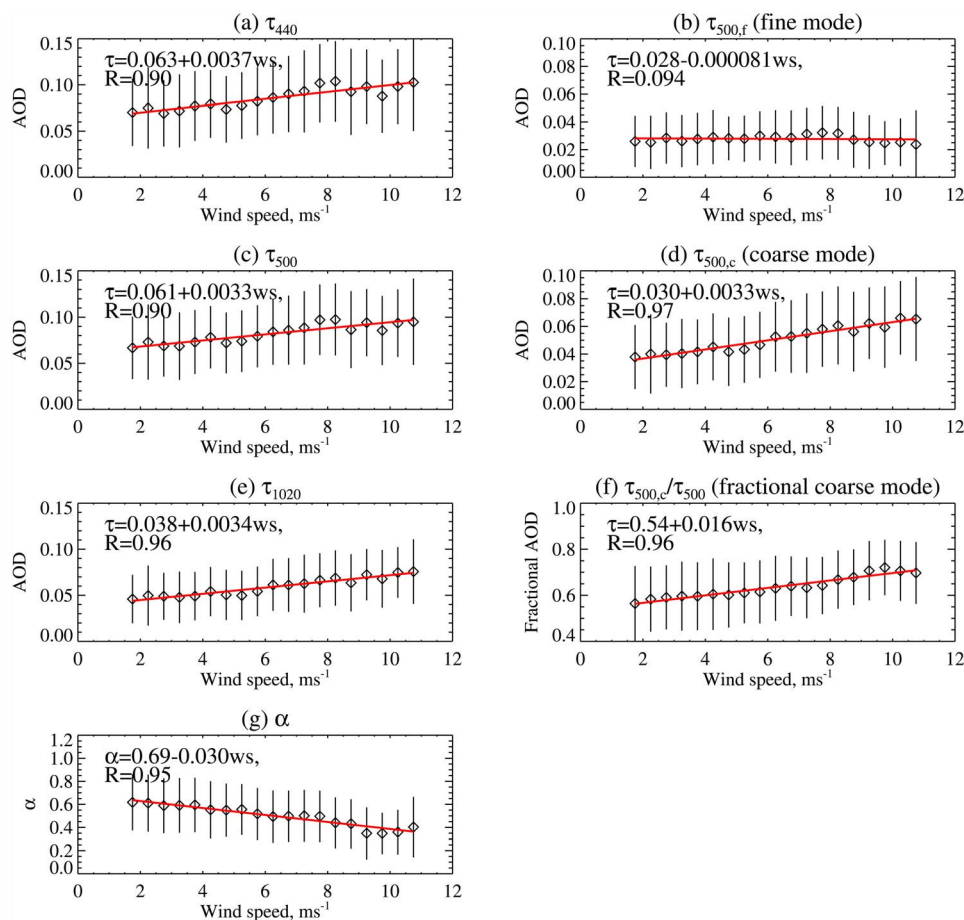


Figure 9. Relationship between daily averages of wind speed and (a, c, e) spectral AOD; (b) fine and (d) coarse-mode contributions to AOD at 500 nm; (f) the fractional contribution of the coarse mode to the total AOD at 500 nm; and (g) α . Data binned by wind speed in bins of 0.5 ms^{-1} . Bin medians are used, and error bars show the standard deviation on each bin's data. Coefficients of linear fit are given in the plots, and illustrated with red lines; R indicates Pearson's linear correlation coefficient. Data are only shown where a bin contains at least 50 data points.

version 2 Optimal Interpolation (OI) SST data set [Reynolds *et al.*, 2006] is used for a joint analysis of effect of wind speed and SST on aerosol. This provides global gap-filled, bias-corrected, daily average (daytime and nighttime orbits) bulk SST. As the SST is bias-corrected against buoys, this bulk SST corresponds to a depth of order 0.5 m below the surface, and is typically within 0.5 K of the skin SST, although this depends on meteorological factors [e.g., Murray *et al.*, 2000]. It is provided on a 0.25° grid but here is downsampled to 2.5° resolution to provide a better representation over the larger source region that the AERONET site may sample from on a given day.

[49] The mean SST is 24.8°C (median 25.0°C), and the standard deviation 2.8°C . The coolest and warmest temperatures encountered are 4.2°C and 31.0°C respectively, although the number of cases with water cooler than 20°C is very small. This is because the majority of the sites are in warm tropical waters, and so any conclusions drawn may be unrepresentative of cooler waters.

[50] Figure 10 is analogous to Figure 7, except the data are also subdivided by SST. The 24-hour-averaged wind speed has been used to stratify the data, although the results do not

change significantly if the instantaneous wind speed is used instead. The SST bins have been chosen to be narrow while still retaining sufficient sampling in as many cases as possible, although this is difficult for the highest wind speeds ($ws > 10 \text{ ms}^{-1}$). Despite the previously-documented links between SST and marine aerosol production, there appears no strong and consistent link with the size distribution here (certainly compared with the effects of wind speed). For high winds, the coolest ($\text{SST} < 21^\circ\text{C}$) and warmest ($\text{SST} > 27^\circ\text{C}$) have a higher coarse-mode volume than the intermediate SST ranges, although the sample size for these wind and SST bins is very limited, so these results should be interpreted with caution.

[51] Jaeglé *et al.* [2011] found that scaling the source function for marine aerosol production by polynomials in SST and wind speed improved the marine aerosol burden in a global chemistry transport model. Regressing aerosol volume jointly against wind speed and SST was also attempted using the AERONET data in this study (not shown), although SST was not found to significantly increase the predictive skill over using wind speed only. This may reflect uncertainties in how well the data sets (AERONET, wind, and SST) are able

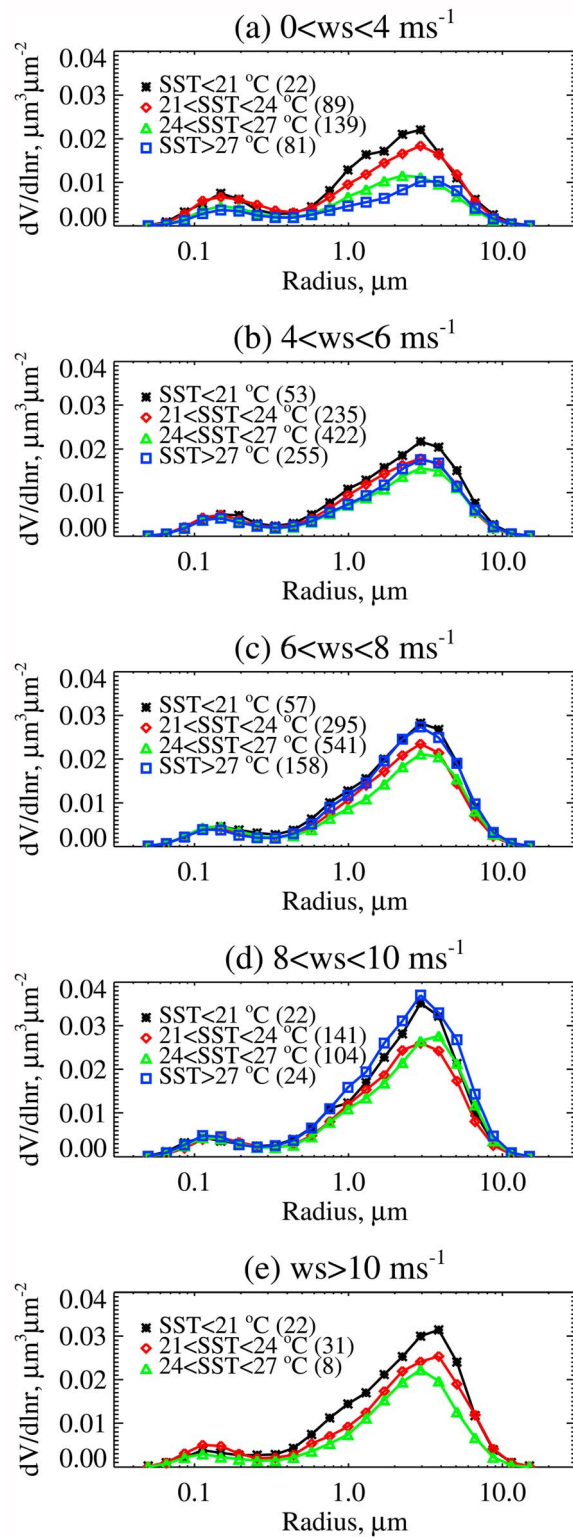


Figure 10. (a–e) Size-bin-median AERONET aerosol volume size distributions, arranged by near-surface 24-hour-averaged wind speed (range indicated above plots), and binned according to the 24-hour-averaged SST. The number of size distribution inversions contributing to each line is given in the legend. Note that Figure 10e contains no points in the warmest SST range.

to represent the true aerosol or meteorological conditions, or simply that aerosol lifetime is sufficiently long that SST has little impact on the total aerosol burden in these regions. The SST range sampled may be a significant factor, given that the largest corrections to the aerosol source function made by Jaeglé *et al.* [2011] are outside the typical range of AERONET data used here.

3.3. Dependence on Relative Humidity

[52] Historically, a common approach to modeling aerosol microphysical properties (e.g., Shettle and Fenn [1979], and those which draw from it) has been to initially define properties for a ‘dry’ aerosol type of some assumed composition. These ‘dry’ properties are then modified according to variations in relative humidity (rh) using models of aerosol swelling [Hänel, 1976; Kotchenruther *et al.*, 1999] for marine cases. With increasing rh , the size distribution shifts to larger particles, and the refractive index approaches that of water. As the size distributions in this work are calculated from AERONET inversions they represent the aerosol size distributions as found ‘in the wild’, and their variability will encompass the effects of the range of relative humidity and consequent aerosol swelling and drying. Several factors complicate the analysis of rh variations. Analogously to wind speed, the quality at which coarse-resolution model relative humidity is able to represent the actual relative humidity on a finer scale is likely highly variable. Aerosol swelling shows hysteresis, such that even if the relative humidity were known this may not be sufficient to model the extent of swelling unless the prior history of the air mass is also known [Kotchenruther *et al.*, 1999]. Additionally, there is evidence that in the case of sea salt aerosol the currently-used mixing rules do not reproduce the observed refractive index [Irshad *et al.*, 2009]. Finally, it should not necessarily be expected that the AOD should correlate well with near-surface humidity, as AOD is a columnar quantity.

[53] NCEP rh data are interpolated here to AERONET inversions in the same way as the wind speed data. There is little direct correspondence between the relative humidity and wind speed (not shown), and the interval $60 \leq rh \leq 80\%$ contains 90% of all relative humidities encountered. Figure 11 shows the averaged AERONET size distribution

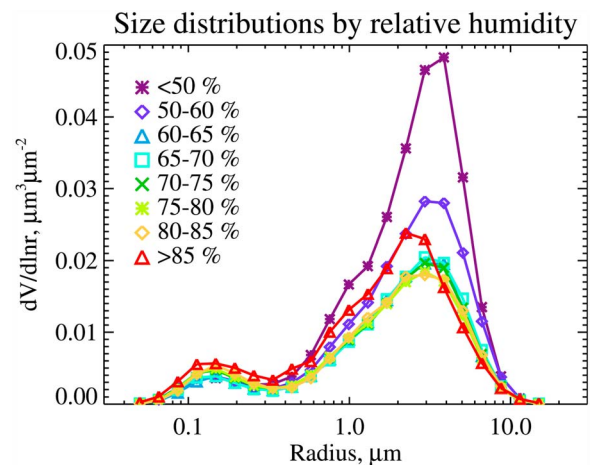


Figure 11. As in Figure 7, except binned by relative humidity.

Table 6. Number of Retrievals, AOD at Three Wavelengths, Ångström Exponent, and Average Wind Speed Corresponding to AERONET Aerosol Volume Size Distributions, Binned as a Function of Near-Surface Relative Humidity^a

Relative Humidity	Number of Retrievals	τ_{440}	τ_{500}	τ_{1020}	α	Wind Speed (ms ⁻¹)
0–50%	4	0.10 (0.021)	0.098 (0.017)	0.082 (0.017)	0.22 (0.10)	5.07
50–60%	67	0.083 (0.026)	0.082 (0.025)	0.058 (0.014)	0.37 (0.20)	6.45
60–65%	265	0.067 (0.019)	0.064 (0.019)	0.043 (0.014)	0.49 (0.21)	6.61
65–70%	697	0.067 (0.022)	0.063 (0.021)	0.043 (0.016)	0.50 (0.17)	6.83
70–75%	882	0.073 (0.024)	0.070 (0.021)	0.045 (0.017)	0.58 (0.18)	6.17
75–80%	575	0.073 (0.022)	0.070 (0.019)	0.046 (0.016)	0.60 (0.19)	5.72
80–85%	189	0.073 (0.026)	0.071 (0.023)	0.044 (0.016)	0.67 (0.16)	5.39
85–100%	18	0.11 (0.040)	0.10 (0.040)	0.069 (0.021)	0.71 (0.19)	5.85

^aFigures in parentheses indicate σ_{med} .

(calculated as previously) for inversions aggregated by relative humidity; Table 6 shows the number of retrievals in each bin, as well as τ , α , and the mean wind speed for the data in that bin (which is similar for each). Table 7 gives statistics of these distributions and fits to them, in the same way as Table 4 for wind speed. To further examine these relationships between relative humidity and AOD for dry and moist air, as with the previous wind speed analysis, linear regressions have been performed using binned direct-Sun and SDA data (Figure 12).

[54] Some studies have observed an anticorrelation of τ and rh for $rh < 75\%$, and a positive correlation for $rh > 75\%$, when measured simultaneously on ships [Smirnov and Shifrin, 1989; Smirnov et al., 1995]. This was attributed to turbulent exchange in the marine boundary increasing τ and decreasing rh , leading to a natural anticorrelation, but this effect being overwhelmed by moisture uptake for high humidities (with a deliquescence point at $rh \approx 75\%$, dependent on temperature and composition). Upon first examination, the AERONET inversions provide some evidence to support this relationship. The AOD and $C_{v,c}$ decrease with increasing rh until around $rh = 60\%$. No inversions had $rh > 90\%$; the highest occupied humidity range (which only contains 18 inversions) does show an increase in volume in both modes (but a drop in $r_{v,c}$). This behavior is consistent with increased turbulence leading to increased particle number (but little change in particle type) in ‘dry’ conditions, and possible aerosol swelling (enhanced volume) in ‘moist’ conditions.

[55] However, the evidence is weak, because of the poor sampling for low and high humidities. For the highest humidities, the fact that these are grid-box average humidities suggests the presence of clouds in some region of the grid box is likely, and so it may be that these distributions are contaminated by clouds. Of the 71 points with $rh < 60\%$, 40 occur at Midway Island, 19 at Lanai, and 6 at Bermuda. This region can on occasion be influenced by transported dust [Smirnov et al., 2000b, 2003b]. It is therefore possible that the low-humidity results here are influenced by dust transported in dry air masses, rather than a change in the abundance of marine aerosol. All of these points at Midway occur from December to April, when dust transport is expected to be most likely. If points from Midway and Lanai are removed, then for $rh < 60\%$ the mean $\tau_{440} = 0.068$, $\tau_{1020} = 0.047$, and $\alpha = 0.38$, although sampling becomes very poor. In these cases the AODs and size distributions for low humidities match closely those for other humidity ranges in Table 6, and the trend in AOD with rh is effectively removed, although the trend in α remains. Removing the Bermuda data does not have a significant effect on the results. It is therefore possible that this small number of the driest cases represent residual contamination by transported dust. The coarse-mode peak radius is also shifted to larger volumes for these drier bins, which supports this (Figure 11). If these seasons are removed for these sites for the analysis in section 2.2, the impact is negligible.

Table 7. As in Table 4, Except for AERONET Distributions Binned as a Function of Relative Humidity

Relative Humidity	$C_{v,f} (\mu\text{m}^3 \mu\text{m}^{-2})$	$C_{v,c} (\mu\text{m}^3 \mu\text{m}^{-2})$	$r_{v,f} (\mu\text{m})$	$r_{v,c} (\mu\text{m})$	σ_f	σ_c	$r_{\text{eff},f} (\mu\text{m})$	$r_{\text{eff},c} (\mu\text{m})$
<i>AERONET Average Parameters</i>								
0–50%	0.0050 (0.0010)	0.073 (0.0090)	0.186 (0.026)	2.49 (0.088)	0.53 (0.013)	0.64 (0.025)	0.162 (0.022)	1.99 (0.056)
50–60%	0.0050 (0.0020)	0.051 (0.011)	0.168 (0.013)	2.49 (0.18)	0.49 (0.031)	0.68 (0.026)	0.149 (0.012)	1.97 (0.15)
60–65%	0.0050 (0.0020)	0.035 (0.012)	0.174 (0.013)	2.40 (0.19)	0.49 (0.027)	0.67 (0.028)	0.154 (0.011)	1.90 (0.15)
65–70%	0.0050 (0.0020)	0.036 (0.011)	0.168 (0.014)	2.46 (0.18)	0.49 (0.026)	0.68 (0.026)	0.149 (0.013)	1.92 (0.14)
70–75%	0.0050 (0.0020)	0.036 (0.011)	0.168 (0.014)	2.46 (0.18)	0.49 (0.026)	0.68 (0.026)	0.149 (0.013)	1.92 (0.14)
75–80%	0.0060 (0.0020)	0.035 (0.012)	0.166 (0.014)	2.38 (0.19)	0.48 (0.026)	0.68 (0.026)	0.148 (0.012)	1.87 (0.14)
80–85%	0.0070 (0.0030)	0.034 (0.014)	0.172 (0.014)	2.38 (0.28)	0.46 (0.024)	0.67 (0.034)	0.155 (0.011)	1.87 (0.21)
85–100%	0.0010 (0.0030)	0.045 (0.014)	0.174 (0.014)	2.21 (0.24)	0.49 (0.050)	0.69 (0.033)	0.148 (0.011)	1.72 (0.16)
<i>Bimodal Fit to Median Distribution</i>								
0–50%	0.0049 (0.00037)	0.070 (0.0050)	0.156 (0.0067)	2.89 (0.15)	0.51 (0.049)	0.62 (0.051)	0.137 (0.0059)	2.39 (0.12)
50–60%	0.0052 (0.00047)	0.048 (0.0026)	0.155 (0.0086)	2.78 (0.12)	0.54 (0.061)	0.69 (0.044)	0.134 (0.0074)	2.19 (0.096)
60–65%	0.0051 (0.00040)	0.035 (0.0019)	0.156 (0.015)	2.57 (0.11)	0.50 (0.028)	0.71 (0.044)	0.138 (0.013)	1.99 (0.088)
65–70%	0.0049 (0.00045)	0.035 (0.0019)	0.153 (0.0082)	2.65 (0.11)	0.51 (0.058)	0.71 (0.043)	0.134 (0.0072)	2.07 (0.089)
70–75%	0.0057 (0.00047)	0.035 (0.0019)	0.153 (0.0070)	2.58 (0.12)	0.49 (0.049)	0.72 (0.046)	0.136 (0.0062)	1.99 (0.090)
75–80%	0.0058 (0.00046)	0.033 (0.0016)	0.155 (0.0068)	2.47 (0.10)	0.49 (0.046)	0.74 (0.042)	0.138 (0.0060)	1.88 (0.079)
80–85%	0.0060 (0.00041)	0.034 (0.0015)	0.160 (0.0057)	2.48 (0.092)	0.47 (0.038)	0.74 (0.037)	0.144 (0.0052)	1.89 (0.070)
85–100%	0.0083 (0.00066)	0.041 (0.0019)	0.163 (0.0082)	2.12 (0.085)	0.57 (0.056)	0.74 (0.041)	0.139 (0.0069)	1.61 (0.064)

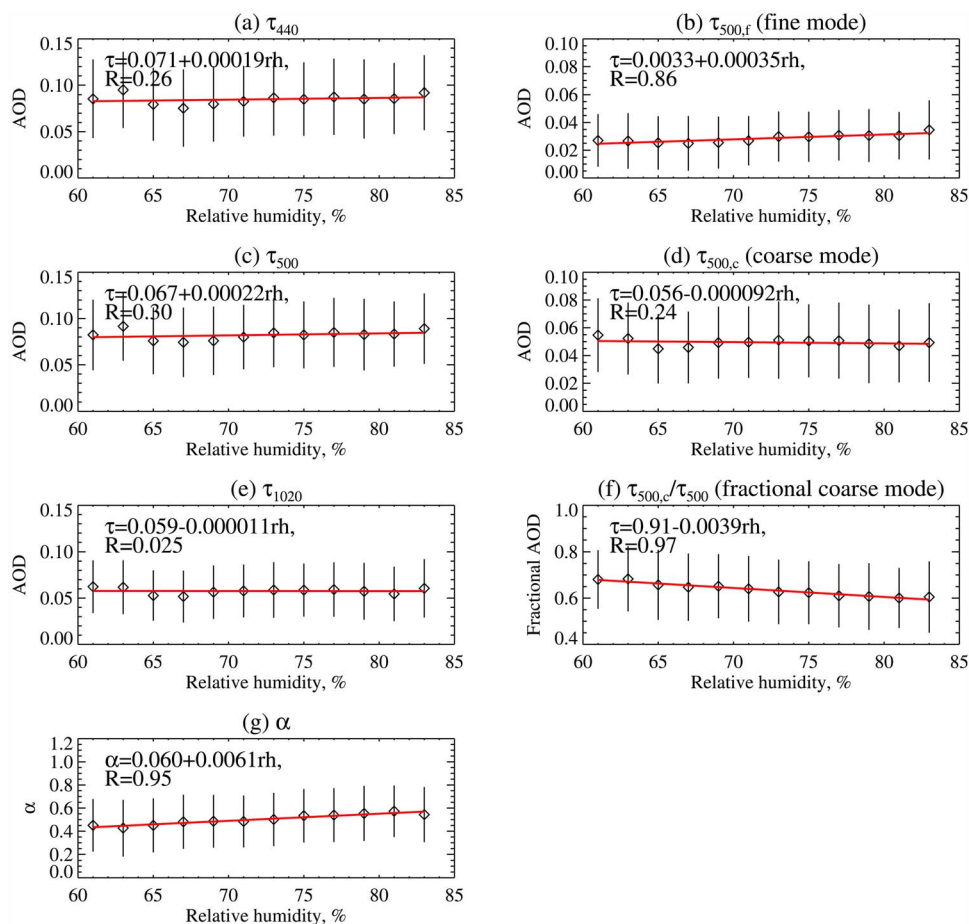


Figure 12. As Figure in 9, except binned by relative humidity. The bin size is 2%.

[56] Over the range of rh with sufficient sampling, the total AOD shows almost no change. For both inversions and direct-Sun data, the variability within each bin is larger than the range spanned by bin-median values. There is, however, a small increase of α with rh . Figure 12 reveals this is driven largely by a small increase in the fine-mode contribution to AOD. The reasons for this behavior are uncertain and it is suggested as a worthwhile avenue for future study. One interpretation is that this could indicate that the fine-mode aerosol swells at lower humidities than the coarse mode.

[57] Some of the variability in all these cases will arise from the hysteresis of aerosol deliquescence (i.e., the path by which the current relative humidity was reached is important), which may mask any change in aerosol properties expected around $rh = 75\%$. Over the heavily-populated range $60 \leq rh \leq 80\%$ size distribution parameters show little change, suggesting that average values are sufficient to describe the majority of cases encountered. The same conclusion is reached if other wavelengths are used; whether the data are subset according to wind speed or not; or whether sites are considered individually or jointly.

3.4. Dependence on Water Vapor Content

[58] In addition to the aerosol bands, the Sun-photometers used in AERONET have a channel around 940 nm which enables the retrieval of water vapor with an uncertainty of order 5%–10% [Smirnov *et al.*, 2004; Alexandrov *et al.*,

2009]. This provides an alternative way to examine the effect of moisture on maritime aerosol. The columnar water vapor is provided in units of g cm^{-2} (equivalent to cm, given a density of 1 g cm^{-3}). Separating the AERONET size distributions according to columnar water vapor gives average distributions shown in Figure 13. The lowest bin

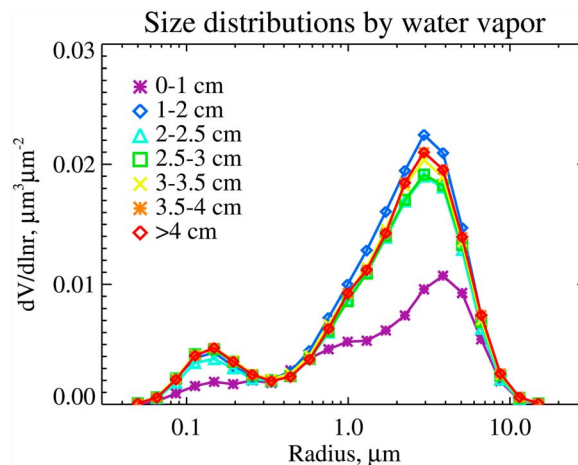


Figure 13. As in Figure 7, except binned by AERONET columnar water vapor amount.

Table 8. Number of Retrievals, AOD at Three Wavelengths, Ångström Exponent, and Average Wind Speed Corresponding to AERONET Aerosol Volume Size Distributions, Binned as a Function of AERONET Columnar Water Vapor^a

Water Vapor	Number of Retrievals	τ_{440}	τ_{500}	τ_{1020}	α	Wind Speed (ms^{-1})
0–1 cm	16	0.036 (0.021)	0.039 (0.029)	0.031 (0.022)	0.48 (0.23)	5.84
1–2 cm	443	0.075 (0.027)	0.072 (0.023)	0.052 (0.019)	0.46 (0.21)	6.68
2–2.5 cm	549	0.067 (0.023)	0.063 (0.020)	0.042 (0.015)	0.51 (0.17)	6.79
2.5–3 cm	670	0.070 (0.022)	0.065 (0.020)	0.043 (0.016)	0.59 (0.19)	6.08
3–3.5 cm	583	0.074 (0.021)	0.070 (0.020)	0.046 (0.016)	0.59 (0.18)	5.94
3.5–4 cm	292	0.071 (0.018)	0.068 (0.018)	0.045 (0.015)	0.62 (0.16)	5.94
4+ cm	144	0.071 (0.020)	0.068 (0.016)	0.043 (0.014)	0.64 (0.19)	5.33

^aFigures in parentheses indicate σ_{med} .

($0 \leq wv \leq 1$ cm) has the lowest volume (and AOD), but aside from that there is no significant dependence the aerosol size distribution on water vapor content. Table 8 shows the variation in AOD with columnar water vapor, along with the average wind speed for each bin; there is no trend. The case of the $0 \leq wv \leq 1$ cm bin is sampled poorly, and seven of the sixteen size distributions are from Crozet Island, so in this case the low AOD and water vapor may both be due to conditions specific to this site, rather than the more general open ocean. There is a small increase of α with water vapor; however, the variability on α within each bin (0.16–0.23) is of similar size to the range over all bins.

[59] The relationship has also been examined for individual sites, and restricted to different subsets of wind speeds, to investigate whether data aggregation decisions result in the signal being masked; no significant relationships were found. The lack of correlation could be explained as a combination of effects resulting from the low ranges of AOD and water vapor encountered; that the vertical distributions of aerosol and water vapor have small overlap thus limited potential for influence; or the possibility that the timescales of aerosol growth and water vapor variability are different. This site-dependent relationship (or lack thereof) between AOD and moisture has been noted in previous studies [Exton *et al.*, 1985; Hoppel *et al.*, 1990; Smirnov *et al.*, 1995, 2000c; Holben *et al.*, 2001; Sakerin *et al.*, 2008].

[60] The strength of the correlation coefficient R between water vapor content and AOD for direct-Sun data is 0.2 or less in most cases when calculated for any site or wavelength, for a selection of assumed relationships (linear, quadratic, or exponential). This is consistent with the results from the smaller AERONET inversion data set. In case the restrictions $\tau_{500} \leq 0.2$ and $0.1 \leq \alpha \leq 1$ were masking a relationship, data without these two constraints have also been examined. The relationships remain weak; an example is shown for Lanai and Midway Island in Figure 14, for exponential fits between wv and τ_{500} (results are similar for other wavelengths, or from the SDA data set). At Midway Island there is evidence that enhanced water vapor corresponds with a decrease in AOD. This could be related to periodic transport of Asian dust in dry air masses [Smirnov *et al.*, 2003b; Eck *et al.*, 2005] rather than an effect of water vapor on marine aerosol. Also shown in Figure 14 are analogous results for the AERONET sites of Wallops (coastal; 37.942°N, 75.475°W) and COVE (a platform 25 km from the coast; 36.900°N, 75.710°W). Because of their coastal (rather than remote) locations they are more susceptible to continental influence, which is reflected in the higher AODs than observed at Lanai or Midway Island. At these sites, for both the ‘all points’ and ‘maritime conditions’ data sets there is a significant strong exponential relationship between AOD and water vapor content, with $R = 0.64 - 0.77$

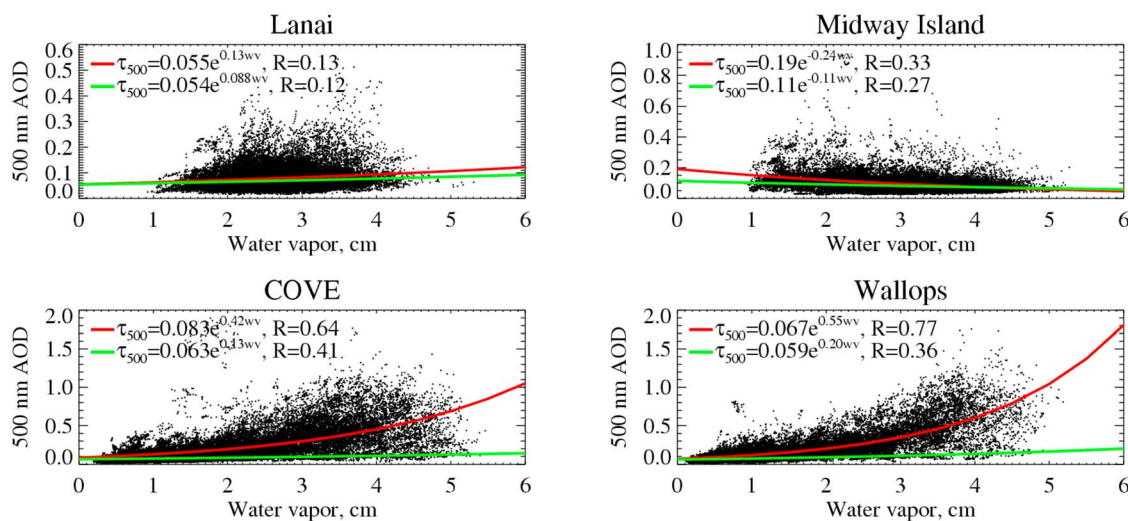


Figure 14. Relationship between water vapor content (wv) and τ_{500} from the AERONET direct-Sun product, for four sites. In each case, the red line indicates an exponential fit to all points, and the green line an exponential fit to only those points where $\tau_{500} \leq 0.2$ and $0.1 \leq \alpha \leq 1$ (deemed maritime conditions). The equation of each fit line, and Pearson's linear correlation coefficient of the fit (R), are given in each plot.

Table 9. Refractive Indices $m = n - ik$ for Marine Aerosol Tested in This Work, Along With Information on Sources

Case	Fine Mode	Coarse Mode	Data Source
1	1.37 - 0.001i	1.37 - 0.001i	<i>Smirnov et al.</i> [2003a]; average of AERONET inversion results for Lanai.
2	1.45 - 0.0035i	1.35 - 0.001i	<i>Remer et al.</i> [2006]; pair of oceanic components used in MODIS collection 5 aerosol retrieval.
3	1.39 - 0.003i	1.39 - 0.003i	<i>Silva et al.</i> [2002]; ground-based unpolluted maritime measurements on the Portuguese coast.
4	1.415 - 0.002i	$1.363 - 3 \times 10^{-9}i$	<i>Shettle and Fenn</i> [1979]/ <i>Hess et al.</i> [1998] at 500 nm and $rh = 70\%$; fine: water soluble component; coarse: accumulation/coarse sea salt component.
5	1.415 - 0.002i	$1.434 - 3 \times 10^{-9}i$	As case 4, except real part of coarse mode from <i>Irshad et al.</i> [2009] infrared laboratory data at $rh = 74.2\%$, retrieval value at 500 nm.

for fits to all points, and $R = 0.36 - 0.41$ for only those classified as maritime conditions, stronger than most of the relationships found for the sites considered for this study. This provides further evidence that the lack of correlation observed for the maritime sites under maritime conditions is real.

3.5. Other Factors

[61] Various studies have shown that the organic content of submicron marine aerosol is increased in waters with high biological activity [*O'Dowd and de Leeuw*, 2007; *Fuentes et al.*, 2010]. *Fuentes et al.* [2010] found, for experiments with seawater proxies enriched with algal species, that the number of generated aerosol particles of modal dry radius of approximately $0.02 \mu\text{m}$ was increased by up to approximately a factor of two as compared to a proxy without the algae. The effect on larger particles (which comprise the more optically-active part of the aerosol size distribution) was smaller. Therefore it is unlikely that this enrichment has a strong effect on the visible AOD. Additional factors influencing marine aerosol production are discussed by *Podzimek* [1980] and *Lewis and Schwartz* [2004], but are either difficult to assess using available data, or likely to have a minor influence on the AOD, and so are not further considered here. These include atmospheric stability, precipitation, surface-active materials (such as the aforementioned organic carbon), wave state, boundary layer height, fetch, salinity, and bottom topography.

4. Refractive Index and Calculated AOD

[62] As well as the size distribution, knowledge of the complex refractive index $m = n - ik$, where n is the real component and k the absorption coefficient, is required to calculate the AOD at a given wavelength. As mentioned previously, the AERONET refractive index retrieved is uncertain at low AOD [*Dubovik et al.*, 2000]. Additionally, the inversion assumes a single refractive index for the aerosol model. Observational evidence suggests that the fine mode is composed largely of sulphates, organic compounds, and salt, while the coarse mode is predominantly salt [*Hegg et al.*, 1997; *Magi et al.*, 2005; *Clarke et al.*, 2006; *O'Dowd and de Leeuw*, 2007; *Fuentes et al.*, 2010]. These different compositions would be expected to lead to different refractive indices for the two modes. For these reasons, a variety of refractive indices are tested in this work, shown in Table 9. This includes ground-based observations, as well as one pair of components used in the current Moderate Resolution Imaging Spectroradiometer (MODIS) AOD retrieval over ocean [*Remer et al.*, 2006], and the Optical Properties of

Aerosol and Clouds (OPAC) database [*Hess et al.*, 1998], which is drawn from *Shettle and Fenn* [1979] and used in various other satellite and model data sets [e.g., *Sayer et al.*, 2010]. This is by no means an exhaustive list, although it does encompass the range of commonly-used values. Although the refractive index has spectral behavior, over the range of interest here most studies in Table 9 use a broadband value, as variation through the visible and near-IR is small.

[63] The refractive indices and size distribution fitting method are tested by attempting to recreate each case of AERONET spectral AOD using Mie theory and the multi-site average size distribution parameters $r_{v,f}$, $r_{v,c}$, σ_f , and σ_c from both fitting methods (Table 2). The distribution volumes $C_{v,f}$ and $C_{v,c}$ for each case are taken from the AERONET-reported parameters (or a lognormal fit to the size distribution, as described previously) for each individual observation. In this way the tests mimics the way the average model may be implemented in satellite retrieval schemes, i.e., the spectral AOD is determined only by altering the volumes of each component while the distribution peak radius and spread are held constant. This allows an assessment of the degree to which the average model is able to represent maritime aerosol at each site, and will inherently include the effects of changes in meteorology and composition.

[64] For each site, the correlation coefficient, median bias (calculated - AERONET observed AOD), and σ_{med} are calculated. The evaluation of each combination of size distribution and refractive index is restricted to only five sites in Table 1 (Lanai, Bermuda, Midway Island, Ascension Island, and Tahiti) which provide a representative data set of maritime aerosol data of reasonable size. Although Nauru has 101 observations, it is omitted due to the previously-discussed suspected influence of surf-generated aerosol [*Henderson et al.*, 2006]. Over this subset of sites, the minimum, maximum, and median of each of these parameters is presented for each case in Figure 15. This provides a simple reference of how well each potential combination of size distribution and refractive index is able to represent the AERONET AOD.

[65] Figure 15 reveals that, in general, the spread of statistics between sites is larger than the spread induced by changes in refractive index. All models tends to overestimate α , due to τ_{440} being comparatively unbiased while the AOD at longer wavelengths has a slight low bias. For the purpose of satellite AOD retrievals, this is not likely to be a problem as the bias could simply be redressed by altering the total volume of the fine and/or coarse modes. However, this would mean that the bias would translate from AOD into volume, which would then mean that derived aerosol mass estimates may be inaccurate.

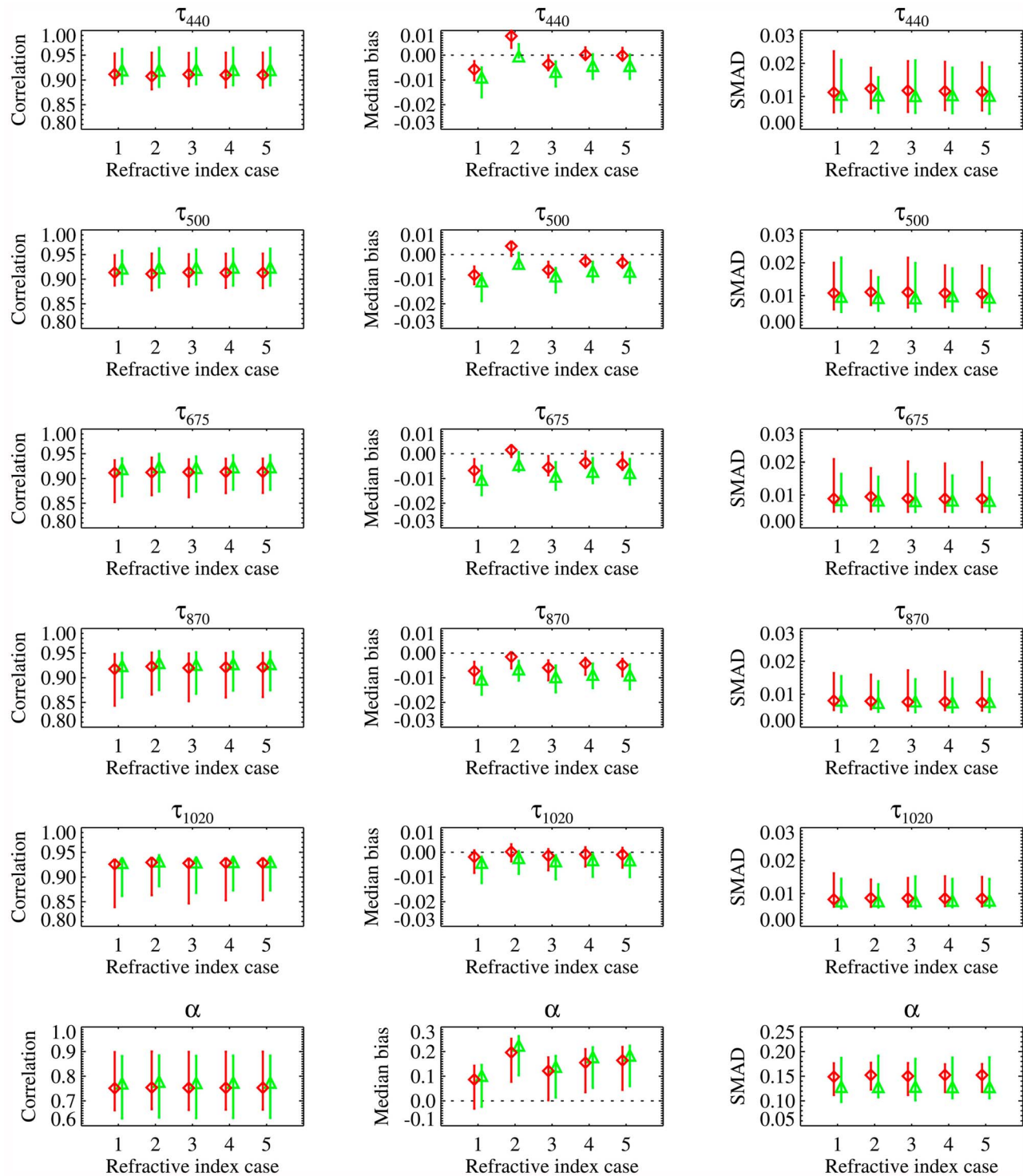


Figure 15. Statistics of comparison of spectral AOD and Ångström exponent between AERONET retrievals, and calculations performed using the average aerosol size distribution parameters, for a variety of assumed aerosol refractive indices (cases in Table 9). Subfigures show (left) Pearson's linear correlation coefficient, (middle) median bias, and (right) σ_{med} . Red diamonds indicate the 'AERONET lognormal' approach and green triangles the 'lognormal fitted' method, slightly offset along the x-axis for clarity. Symbols show the median, and error bars the minimum and maximum values, over the ensemble of five sites used for the evaluation.

Table 10. Pearson's Linear Correlation Coefficient (top portion), Median (Calculated-AERONET Observed) Bias (middle portion), and σ_{med} (Bottom Portion) Between Observed AERONET Spectral AOD and Ångström Exponent, and That Calculated Using the Average "Lognormal Fitted" Fine and Coarse Mode Radii and Spreads for Refractive Index Case 4 From Table 9

Site	τ_{340}	τ_{380}	τ_{440}	τ_{500}	τ_{675}	τ_{870}	τ_{1020}	α
<i>Correlation Coefficient</i>								
Lanai	0.94	0.95	0.96	0.95	0.94	0.93	0.93	0.75
Bermuda	0.89	0.90	0.90	0.90	0.87	0.86	0.85	0.74
Kaashidhoo	0.88	0.89	0.90	0.89	0.87	0.86	0.85	0.86
Midway Island	0.90	0.90	0.91	0.91	0.91	0.92	0.94	0.90
Ascension Island	0.88	0.89	0.88	0.88	0.87	0.87	0.89	0.87
Tahiti	0.89	0.90	0.95	0.93	0.94	0.95	0.93	0.66
Amsterdam Island	0.95	0.95	0.95	0.95	0.95	0.95	0.96	0.79
Crozet Island	0.94	0.95	0.95	0.93	0.93	0.96	0.94	0.079
Guam	0.80	0.80	0.79	0.80	0.80	0.76	0.76	0.79
Nauru	0.87	0.88	0.89	0.87	0.88	0.86	0.86	0.84
Graciosa	0.85	0.87	0.88	0.88	0.88	0.89	0.90	0.77
<i>Median Bias</i>								
Lanai	0.0038	0.0040	0.0029	-0.00055	0.00053	-0.0035	0.0018	0.16
Bermuda	-0.0020	-0.000014	-0.00014	-0.0033	-0.0046	-0.0049	-0.0049	0.16
Kaashidhoo	-0.028	-0.026	-0.017	-0.021	-0.019	-0.016	-0.016	0.14
Midway Island	0.0043	-0.00062	0.0030	-0.00088	-0.0042	-0.0060	0.0014	0.22
Ascension Island	0.00031	-0.0018	-0.00031	-0.0046	-0.0065	-0.0094	-0.0062	0.21
Tahiti	-0.010	-0.00099	-0.0013	-0.0040	-0.00091	-0.0023	-0.00095	0.045
Amsterdam Island	0.0042	-0.0014	-0.0019	-0.0050	-0.0034	-0.0090	-0.0059	0.22
Crozet Island	-0.010	-0.0090	-0.011	-0.0083	-0.0050	-0.011	-0.013	0.21
Guam	0.010	0.0080	0.0054	-0.00047	-0.00019	-0.0027	-0.00064	0.14
Nauru	-0.0012	-0.0027	0.00070	-0.0029	-0.0022	-0.0022	-0.0018	0.039
Graciosa	-0.013	-0.0080	-0.014	-0.013	-0.015	-0.015	-0.010	0.25
<i>Scaled Median Absolute Difference</i>								
Lanai	0.012	0.0090	0.0068	0.0065	0.0065	0.0057	0.0061	0.15
Bermuda	0.020	0.020	0.020	0.019	0.020	0.017	0.015	0.17
Kaashidhoo	0.013	0.012	0.0095	0.0010	0.0077	0.0080	0.0084	0.15
Midway Island	0.016	0.014	0.012	0.011	0.0088	0.0075	0.0085	0.12
Ascension Island	0.020	0.019	0.018	0.016	0.014	0.013	0.011	0.13
Tahiti	0.012	0.0075	0.0057	0.0069	0.0049	0.0050	0.0061	0.17
Amsterdam Island	0.0074	0.0073	0.0072	0.0094	0.0081	0.0097	0.0058	0.11
Crozet Island	0.011	0.018	0.015	0.018	0.0087	0.0072	0.0055	0.073
Guam	0.014	0.014	0.011	0.0010	0.0067	0.0068	0.0075	0.12
Nauru	0.0094	0.0082	0.0084	0.0094	0.0066	0.0089	0.0077	0.14
Graciosa	0.017	0.016	0.018	0.018	0.018	0.017	0.018	0.15

[66] The 'fitted lognormal' approach results in higher correlations between calculated and AERONET AOD, with a lower spread of difference (σ_{med}). The correlation coefficients are high in all cases, particularly considering that the range of AOD is small (most data are for $0.03 \leq \tau \leq 0.08$). In contrast, this method leads to slightly more negative biases in AOD. These biases typically remain smaller than σ_{med} , and importantly both of these are often around the reported uncertainty on AERONET AOD of 0.01–0.02 [Holben *et al.*, 1998; Eck *et al.*, 1999]. Here, σ_{med} is the metric of most interest because it provides information on the scatter of the AOD about this bias. For these reasons, the 'fitted lognormal' method is deemed the more useful of the two approaches. This is an important result because it demonstrates that, just by varying the volume of each component, a single value of each of $r_{v,f}$, $r_{v,c}$, σ_f , and σ_c are able to reproduce the AERONET AOD over a variety of oceans, wind speeds, and humidities, with a precision similar to that of the AERONET AOD measurements themselves, and even considering the fact there may be a non-maritime contribution to the aerosol loading in some cases.

[67] There is no clear 'best case' of refractive indices to choose. Biases in the model fit are similar for the longer

wavelengths, where the coarse mode contributes comparatively more to the AOD, which implies that choice of refractive index is probably not significant for the coarse mode. Conversely, for the fine mode those cases with a larger refractive index (2, 4, and 5) result in a higher AOD at 440 nm and 500 nm, which also means they overestimate α more strongly. Given the low AODs encountered, this overestimate of α is not considered problematic, as large errors in α can propagate from small errors in AOD [Wagner and Silva, 2008]. Unfortunately, the AOD is not measured at longer wavelengths at these sites, which means the applicability of the model at other common satellite wavelengths (such as 1.6 μm and 2.1 μm) may not be assessed directly.

[68] Based on these factors, from this point case 4 from Table 9 (fine mode $m = 1.415 - 0.002i$, coarse mode $m = 1.363 - 3 \times 10^{-9}i$) is used, although results are similar if cases 2 or 5 are chosen instead. The correlation, median bias, and σ_{med} for each site for this choice of refractive index, and the recommended 'lognormal fitted' distribution approach, are provided for τ_λ and α in Table 10. These refractive indices (with size distribution component parameters $r_{v,f} = 0.157 \mu\text{m}$, $r_{v,c} = 2.59 \mu\text{m}$, $\sigma_f = 0.50$, $\sigma_c = 0.72$) are hereafter referred to as the 'recommended maritime

Table 11. Comparison Between Spectral AOD and α Modeled Using NCEP Wind Speed and That Measured on MAN Cruises^a

Parameter	Number of Matches	Correlation Coefficient	Median Bias	σ_{med}	Minimum MAN Value	Maximum MAN Value	Fraction Within 0.02
τ_{440}	43	0.50	0.006	0.017	0.032	0.125	0.67
τ_{500}	69	0.42	−0.002	0.021	0.026	0.129	0.62
τ_{675}	69	0.46	0.002	0.019	0.018	0.106	0.67
τ_{870}	69	0.54	−0.0001	0.021	0.017	0.113	0.65
α	69	0.17	0.24	0.331	−0.053	1.163	–

^aThe correlation coefficient is Pearson's linear correlation coefficient, and the bias is defined such that positive values mean the model is larger than the MAN data. The final column shows, for spectral AOD, the fraction of predicted AODs lying within the Sun-photometer typical uncertainty of ± 0.02 .

model'. The single scatter albedo is approximately 0.98 over this wavelength range.

[69] The site with the most negative bias in AOD (for all refractive index cases) is Kaashidhoo; however, as discussed previously, this site is subject to potential seasonal influences of aerosol outflow from the Indian subcontinent, and so likely less representative of clean maritime conditions. The next-largest biases are for Graciosa, which may also potentially be influenced by transported or local pollution. For both of these sites it is likely that a pollutant would be more absorbing than the background maritime aerosol, such that the maritime model would underestimate the fine-mode absorption AOD, which is consistent with the observed underestimates. The small sample size (8) and low AOD mean that α is reconstructed poorly at Crozet Island.

[70] The calculations have also been performed (and included in Table 10) for AOD at 340 nm and 380 nm which, although not used for the AERONET inversion, are available for parts of the record. They are very similar to those at 440 nm, with spectral trends continued (e.g., stronger negative biases at Kaashidhoo). No additional insight into the most suitable refractive index is obtained. Additionally, when shorter wavelengths are considered the assumption of a spectrally-neutral refractive index is also likely less appropriate.

5. Prediction of Maritime Aerosol Network AOD

[71] The previous sections have focussed on coastal island sites. The Maritime Aerosol Network (MAN) component of AERONET [Smirnov et al., 2009] provides spectral AOD measured on ocean cruises using hand-held Microtops II Sun-photometers, with an uncertainty of approximately 0.02 [Knobelspiesse et al., 2004]. The AOD is reported at 440, 500, 675, and 870 nm for the cruises used here. Using these data helps to establish the utility of the wind-speed-dependent relationships observed in previous sections. For this analysis, level 2.0 (cloud-screened and quality-assured) AODs from the 'series-average' product are used. One measurement series is defined in this product as the set of AOD measurements taken with a gap of no more than 2 minutes between an individual pair.

[72] A subset of cruises whose measurements took place in areas likely to have minimal influence from transported aerosol sources are analyzed here. These are the SA Agulhas (during 2007–2008), Marion Dufresne (a cruise from each of 2008, 2009, and 2010), Melville (one in 2010 and two in 2011), and Prince Albert (during 2010). The MAN data are subject to the $\tau_{500} \leq 0.2$ criterion to improve the likelihood that the aerosol sampled is pure maritime in origin; because

of the larger uncertainty on MAN AODs than those from the on-land AERONET sites, the range of permitted Ångström exponents is extended to $-0.1 \leq \alpha \leq 1.2$. Many points remain in coastal or continental outflow regions, such that some contamination by a non-maritime component is likely. To reduce this, it is further required that the measurement be at least 5° from land. This leaves 69 potential cases for comparison (only 43 include AOD at 440 nm).

[73] Next the recommended aerosol size distribution parameters and refractive index as outlined above ($r_{v,f} = 0.157 \mu\text{m}$, $r_{v,c} = 2.59 \mu\text{m}$, $\sigma_f = 0.50$, $\sigma_c = 0.72$, fine mode $m = 1.415 - 0.002i$, coarse mode $m = 1.363 - 3 \times 10^{-9}i$) are used with the relationships $C_{v,f} \approx 0.0057$, $C_{v,c} \approx 0.0079 + 0.0047ws$ to predict the MAN AOD and α . Statistics of the resulting comparison are shown in Table 11, and a scatter plot in Figure 16. Correlation coefficients are between 0.42 and 0.54 for spectral AOD, which, although low, are significant at greater than the 95% level, and reflect the low range of AODs compared with the MAN uncertainty, as well as the high variability of aerosol volume within a single narrow wind speed bin in Figure 8. σ_{med} is also of similar magnitude to the uncertainty in MAN AOD. Because of all these reasons, α is poorly-reproduced. The majority of predicted AODs are within the MAN uncertainty. The wind-speed relationship tends to slightly underestimate

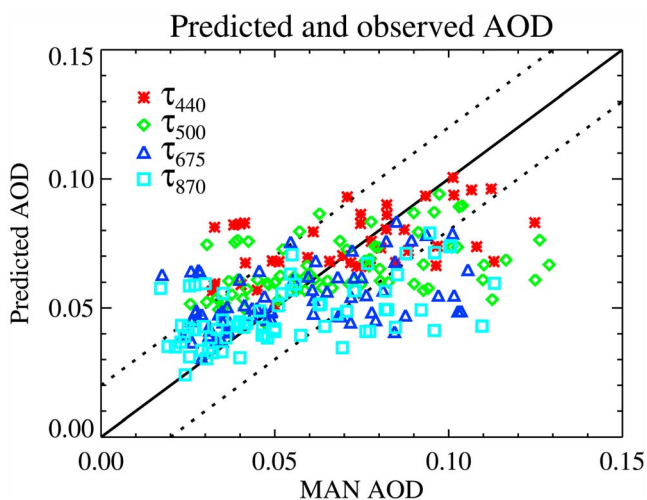


Figure 16. Comparison between MAN AODs and those predicted using the wind-speed relationship from AERONET sites ($C_{v,f} \approx 0.0057$, $C_{v,c} \approx 0.0079 + 0.0047ws$). The solid line is the 1:1 line, and the dotted lines indicate the MAN uncertainty of ± 0.02 .

Table 12. Lidar Ratios S for Unpolluted Marine Aerosol Calculated for 355 nm, 532 nm, and 1064 nm^a

Distribution	Lidar Ratio S		
	355 nm	532 nm	1064 nm
<i>Bimodal Lognormal Fits</i>			
Recommended model	34.2	28.0	30.6
0–4 ms ^{−1}	39.2	33.4	33.9
4–6 ms ^{−1}	35.1	29.3	31.5
6–8 ms ^{−1}	32.4	27.0	29.9
8–10 ms ^{−1}	30.4	25.2	28.7
10+ ms ^{−1}	27.5	24.3	30.2
<i>Exact Size Distributions</i>			
Lanai	33.4	30.3	33.3
0–4 ms ^{−1}	38.8	35.0	35.0
4–6 ms ^{−1}	34.2	31.3	33.6
6–8 ms ^{−1}	31.5	29.3	32.9
8–10 ms ^{−1}	29.6	28.1	32.2
10+ ms ^{−1}	28.7	28.2	33.3

^aThe top section presents results for bimodal lognormal distribution fits. The bottom section presents calculations for the exact averaged size distributions.

AOD for cases of high MAN AOD. Possible reasons for this could be a stronger wind-AOD relationship over the open ocean than at the AERONET sites; that the NCEP data is of different quality over the open ocean as compared to the island sites; or that some of these MAN observations have a residual non-marine aerosol component. An alternative could be differences between the aerosol properties for coastal and open-ocean regions, although this cannot be assessed as the MAN record does not permit retrievals of aerosol size distribution. Performance is similar if the other relationships between wind speed and volume from section 3.2.1 are applied instead (not shown). The main conclusion from this is to confirm that the wind speed alone is not able to predict the instantaneous aerosol burden well over the world's oceans, although it can provide a typical background value.

6. Lidar Ratios

[74] Lidar provide a useful tool for examining the vertical structure of aerosols and clouds, which is not readily accessible from radiometers to the same extent. To convert the backscattering measured by a lidar from a particular altitude range into extinction, the lidar ratio S , which is a function of aerosol type and wavelength, is required. This can be calculated as

$$S_{\lambda} = \frac{\int_0^{\pi} P_{\lambda}(\theta) d\theta}{P_{\lambda}(\pi) \omega_0} \quad (9)$$

where P , the scattering phase function, is typically normalized to integrate to either 1 or 4π , and ω_0 is the aerosol single scattering albedo; i.e., S is simply the ratio of total extinction to backscatter. As such for a given vertically-integrated backscatter, the calculated AOD is directly proportional to S . Depending on the characteristics of an individual lidar, S is either calculated from measured extinction and backscatter (for example, *Pedró et al.* [2010]), or prescribed as a function of aerosol type. In the latter situation the choice of an appropriate S is therefore important for the accurate

calculation of aerosol loading. The Cloud-Aerosol Lidar with Orthogonal Polarisation (CALIOP) sensor has flown as part of the A-Train satellite constellation since 2006, and measures backscattered radiation at 532 nm and 1064 nm (as well as depolarization at 532 nm); the lidar ratios used in the current processing are given by *Omar et al.* [2009]. For unpolluted marine aerosol, these are 20 at 532 nm and 45 at 1064 nm. *Cattrall et al.* [2005, Table 3] provide a summary of some results from the literature, with mid-visible S for marine aerosol between 24 and 39. Their results also show little spectral dependence. *Ackermann* [1998] performed calculations based on the OPAC database, giving S in the range 25–30 at 532 nm and 40–60 at 1064 nm for typical relative humidities. *Müller et al.* [2007] summarize a set of field campaigns, in which S at 532 nm was found to be from 23–29 for marine aerosol. *Pedró et al.* [2010] obtained median values of S at 532 nm of 31, 36, and 37 for air masses originating from different oceanic regions, although there may have been a local contribution to these results. The AERONET analysis of *Smirnov et al.* [2003a] at Lanai gives 34.5 at 500 nm and 37 at 1020 nm.

[75] Lidar ratios from distributions obtained in this study are presented in Table 12 for the commonly-used wavelengths of 532 nm and 1064 nm, and are in the range 25–35. Results are also presented for 355 nm, which will be measured by the forthcoming European Space Agency EarthCARE satellite (although note that this wavelength is somewhat outside the range of the AERONET measurements used to constrain the model). Because the bimodal lognormal fits do not reproduce perfectly the retrieved AERONET size distributions, two sets of calculations are presented. All of these assume the refractive index $m = 1.415 - 0.002i$ (fine mode) and $m = 1.363 - 3 \times 10^{-9}i$ (coarse mode). The first set uses the bimodal lognormal distribution parameters for the recommended aerosol model (section 4), together with bimodal lognormal fits for the distributions binned by wind speed (lower part of Table 4). The second uses the averaged size distributions directly, rather than lognormal fits to them. This makes the assumptions that the volume of particles outside the range of the bins is negligible (supported by Figure 3), and that the cutoff radius between fine and coarse mode (to determine which refractive index to use) is $0.4 \mu\text{m}$, which is close to the inflection point in Figure 3. If the cutoff radius is changed in the region $0.3 \leq r \leq 0.5 \mu\text{m}$, S changes by approximately 1%, so sensitivity to this assumption is small. Additionally, as the recommended model was determined by the weighted average of lognormal fit parameters (rather than a fit to a weighted spectrum), results for Lanai are included in this second case (see Figure 4), as the site with the best sampling. This latter method is expected to yield more accurate lidar ratios, as it uses the retrieved size distributions directly.

[76] Use of exact distributions rather than lognormal fits result in lidar ratios higher by approximately 10% at both 532 and 1064 nm. This difference is due to the fact that the size distributions are not perfectly bimodal lognormal. The results are in good agreement with the ranges of the previously-cited studies; they are, however, significantly higher at 532 nm (lower at 1064 nm) than the values used in CALIOP processing (20 at 532 nm and 45 at 1064 nm [*Omar et al.*, 2009]). This is an important result as applying a lidar ratio of 30 as opposed to 20 for CALIOP at 532 nm

Table 13. Parameters for Recommended Aerosol Model of Unpolluted Marine Aerosol, for Use in General Satellite Remote Sensing Applications^a

Parameter	Value
<i>Fine Mode</i>	
$r_{n,f}$	0.074 μm
$r_{v,f}$	0.157 μm
$r_{\text{eff},f}$	0.139 μm
σ_f	0.50
m	1.415 – 0.002 <i>i</i>
<i>Coarse Mode</i>	
$r_{n,c}$	0.55 μm
$r_{v,c}$	2.59 μm
$r_{\text{eff},c}$	2.00 μm
σ_c	0.72
m	1.363 – $3 \times 10^{-9}i$

^aDefinitions of the size distribution parameters are given in the Introduction (in particular, equation (6)) and Appendix A.

would increase the unpolluted marine aerosol loading by 50%; this would explain the relative low bias of CALIOP marine AODs at 532 nm as compared to other data sets [Kiliyanpilakkil and Meskhidze, 2011; Oo and Holz, 2011]. The difference at 1064 nm is of similar magnitude but opposite sense (i.e., CALIOP lidar ratio around 50% larger than the results here suggest). There is a slight decrease of lidar ratio with wind speed; the change is typically 10% or less from the average value. This provides an estimate of the error which would arise from the assumption of a wind-speed-independent lidar ratio.

[77] If $m = 1.37 - 0.001i$ is used (as in Smirnov *et al.* [2003a]), S increases by approximately 10% at 532 nm and less at 1064 nm. The highlights the sensitivity to the assumed refractive index. Additionally, the AERONET retrievals do not provide information on the vertical profile of the aerosol, provided a column-integrated amount. Therefore a strong vertical inhomogeneity in particle number or size may lead to errors in the retrieved size distributions, and influence the calculated S . Conversely, if there is significant vertical inhomogeneity in the aerosol size distribution or composition, the assumption of vertically-constant S will be inappropriate when trying to estimate total extinction from a lidar.

7. Conclusions

[78] When aerosol size distributions retrieved at 11 island AERONET sites spread throughout global oceans are filtered to extract data likely representative of pure (unpolluted) maritime aerosol, the resulting size distributions are similar, with the chief differences between sites being in the total fine and coarse mode volumes. An aerosol model with size distribution parameters and refractive index shown in Table 13 was found to be able to reconstruct the AERONET AOD with error of order 0.01–0.02, if only the fine and coarse mode volumes are taken as input. This uncertainty is similar to that of the AERONET AOD measurements themselves, and holds at most sites and wavelengths between 340 nm and 1020 nm. These parameters are therefore suggested for use in aerosol remote sensing algorithms to represent unpolluted marine aerosol. The method of performing a bimodal lognormal fit to averaged AERONET size distributions, rather than taking the average of AERONET

retrieved size distribution parameters directly, was found to perform better.

[79] Size distributions are dependent on the wind speed, with higher winds leading to an increased coarse mode total volume and volume mean radius. As the majority of the data are for wind speeds between 4 and 8 ms^{-1} , however, the global average coarse-mode radius can be used in most situations. The fine mode is comparatively unaffected. The AOD and Ångström exponent also show an approximately linear relationship with wind speed. However, correlations are poor unless fits are performed to binned data, underlying the fact that wind speed alone is a poor predictor of the marine aerosol burden. Relative humidity has also been investigated, although poor sampling and potential for influence of transported dust or cloud contamination for the lowest and highest humidities limit the strength of any conclusions which can be drawn. For the 90% of the data within $60 \leq rh \leq 80\%$ there is little change in size distribution parameters. Similarly, SST and columnar water vapor have not been found to have a strong impact on aerosol size distribution parameters, within the ranges sampled.

[80] Lidar ratios calculated from the results in this work give results approximately 50% higher than those used for operational CALIOP algorithm at 532 nm, but more consistent with those from many other studies, consistent with an underestimate of marine AOD by CALIOP as observed in other studies.

Appendix A: Relation Between Number and Volume Size Distributions

[81] For individual lognormal components, the relationships between the volume and number distribution parameters may be calculated using equations (2) and (6) by first noting that (dropping subscripted i)

$$\frac{dV(r)}{d\ln(r)} = \frac{4\pi r^3}{3} \frac{Cn}{\sqrt{2\pi}\sigma} e^{-\frac{1}{2}\left(\frac{\ln(r) - \ln(r_n)}{\sigma}\right)^2} = \frac{4\pi}{3} \frac{Cn}{\sqrt{2\pi}\sigma} e^{-\frac{1}{2}\left(\frac{\ln(r) - \ln(r_n)}{\sigma}\right)^2 + 3\ln(r)}, \quad (\text{A1})$$

then expanding the exponential term

$$\begin{aligned} & -\frac{1}{2} \left(\frac{\ln(r) - \ln(r_n)}{\sigma} \right)^2 + 3\ln(r) \\ & = -\frac{1}{2\sigma^2} [\ln^2(r) - 2\ln(r_n)\ln(r) + \ln^2(r_n) - 6\sigma^2\ln(r)], \end{aligned} \quad (\text{A2})$$

multiplying equation (A1) by

$$1 = e^{3\ln(r_n) + 4.5\sigma^2} e^{-3\ln(r_n) - 4.5\sigma^2} \quad (\text{A3})$$

and combining the second exponential factor in equation (A3) with equation (A2) to give

$$-\frac{1}{2\sigma^2} [\ln^2(r) - 2\ln(r_n)\ln(r) + \ln^2(r_n) - 6\sigma^2\ln(r) + 6\sigma^2\ln(r_n) + 9\sigma^4], \quad (\text{A4})$$

which simplifies to

$$-\frac{1}{2} \left(\frac{\ln(r) - [\ln(r_n) + 3\sigma^2]}{\sigma} \right)^2. \quad (\text{A5})$$

From this the definition

$$\ln(r_v) = \ln(r_n) + 3\sigma^2 \quad (\text{A6})$$

leads to the result that

$$r_v = r_n e^{3\sigma^2}, \quad (\text{A7})$$

and, returning to equation (A1) with the remaining first exponential factor from equation (A3),

$$\begin{aligned} \frac{dV(r)}{d\ln(r)} &= \frac{4\pi}{3} \frac{C_n}{\sqrt{2\pi\sigma}} e^{3\ln(r_n) + 4.5\sigma^2} e^{-\frac{1}{2}\left(\frac{\ln(r) - \ln(r_v)}{\sigma}\right)^2} \\ &= \frac{4\pi}{3} r_n^3 e^{4.5\sigma^2} \frac{C_n}{\sqrt{2\pi\sigma}} e^{-\frac{1}{2}\left(\frac{\ln(r) - \ln(r_v)}{\sigma}\right)^2}, \end{aligned} \quad (\text{A8})$$

hence

$$C_v = \frac{4\pi}{3} r_n^3 e^{4.5\sigma^2} C_n. \quad (\text{A9})$$

[82] **Acknowledgments.** This work was supported by a grant from the NASA MEaSUREs program, managed by M. Maiden. The authors would like to acknowledge Hal Maring for his support of the AERONET program. The AERONET (C. McClain, R. Frouin, J. Sciare, M. A. Lander, R. Wagener) and MAN (S. Piketh, R. Losno, J. Sciare, N. Nelson, K. Voss, R. Frouin, G. Milinevsky) Pls are thanked for the creation and maintenance of the Sun-photometer data sets. G. König-Langlo and the Alfred Wegener Institute for Polar and Marine Research are thanked for the meteorological data from RV Polarstern. NCEP data were obtained from the SeaWiFS Ocean Biology Processing Group data distribution service. The authors are grateful to A. Sinyuk for assistance in verification of the results of Mie computations, and S. Kinne and two anonymous reviewers for their comments and suggestions, which helped us to improve the manuscript.

References

- Ackermann, J. (1998), The extinction-to-backscatter ratio of tropospheric aerosol: A numerical study, *J. Atmos. Oceanic Technol.*, **15**, 1043–1050.
- Adames, A. F., M. Reynolds, A. Smirnov, D. S. Covert, and T. P. Ackerman (2011), Comparison of MODIS ocean aerosol retrievals with ship-based Sun photometer measurements from the Around the Americas expedition, *J. Geophys. Res.*, **116**, D16303, doi:10.1029/2010JD015440.
- Ahmad, Z., B. A. Franz, C. R. McClain, E. J. Kwiatowska, J. Werdell, E. P. Shettle, and B. N. Holben (2010), New aerosol models for the retrieval of aerosol optical thickness and normalized water-leaving radiances from the SeaWiFS and MODIS sensors over coastal regions and open oceans, *Appl. Opt.*, **49**(29), 5545–5560, doi:10.1364/AO.49.005545.
- Alexandrov, M. D., B. Schmid, D. D. Turner, B. Cairns, V. Oinas, A. A. Lacis, S. I. Gutman, E. R. Westwater, A. Smirnov, and J. Eilers (2009), Columnar water vapor retrievals from multifilter rotating shadowband radiometer data, *J. Geophys. Res.*, **114**, D02306, doi:10.1029/2008JD010543.
- Ångström, A. (1929), On the atmospheric transmission of Sun radiation and on dust in the air, *Geogr. Ann.*, **12**, 130–159.
- Angelova, M., and F. Webster (2006), Whitecap coverage from satellite measurements: A first step toward modeling the variability of ocean whitecaps, *J. Geophys. Res.*, **111**, C03017, doi:10.1029/2005JC003158.
- Blanchard, D. C., and A. H. Woodcock (1980), The production, concentration, and vertical distribution of the sea-salt aerosol, *Ann. N. Y. Acad. Sci.*, **338**, 330–347, doi:10.1111/j.1749-6632.1980.tb17130.x
- Cattrell, C., J. Reagan, K. Thome, and O. Dubovik (2005), Variability of aerosol and spectral lidar and backscatter and extinction ratios of key aerosol types derived from selected Aerosol Robotic Network locations, *J. Geophys. Res.*, **110**, D10S11, doi:10.1029/2004JD005124.
- Clarke, A. D., S. R. Owens, and J. Zhou (2006), An ultrafine sea-salt flux from breaking waves: Implications for cloud condensation nuclei in the remote marine atmosphere, *J. Geophys. Res.*, **111**, D06202, doi:10.1029/2005JD006565.
- Derber, J. C., D. F. Parrish, and S. Lord (1991), The new global operational analysis system at the National Meteorological Center, *Weather Forecasting*, **6**, 538–547.
- Dubovik, O., and M. D. King (2000), A flexible inversion algorithm for retrieval of aerosol optical properties from Sun and sky radiance measurements, *J. Geophys. Res.*, **105**(D16), 20,673–20,696.
- Dubovik, O., A. Smirnov, B. N. Holben, M. D. King, Y. J. Kaufman, T. F. Eck, and I. Slutsker (2000), Accuracy assessments of aerosol optical properties retrieved from aerosol robotic network (AERONET) Sun and sky radiance measurements, *J. Geophys. Res.*, **105**(D8), 9791–9806.
- Dubovik, O., B. Holben, T. F. Eck, A. Smirnov, Y. Kaufman, M. King, D. Tanré, and I. Slutsker (2002), Variability of absorption and optical properties of key aerosol types observed in worldwide locations, *J. Atmos. Sci.*, **59**, 590–608.
- Dubovik, O., et al. (2006), The application of spheroid models to account for aerosol particle non-sphericity in remote sensing of desert dust, *J. Geophys. Res.*, **111**, D11208, doi:10.1029/2005JD006619.
- Dubovik, O., M. Herman, A. Holdak, T. Lapyonok, D. Tanré, J. L. Deuzé, F. Ducos, A. Sinyuk, and A. Lopatin (2011), Statically optimized inversion algorithm for enhanced retrieval of aerosol properties from spectral multi-angle polarimetric satellite observations, *Atmos. Meas. Tech.*, **4**, 975–1018, doi:10.5194/amt-4-975-2011.
- Eck, T. F., B. N. Holben, J. S. Reid, O. Dubovik, A. Smirnov, N. T. O'Neill, I. Slutsker, and S. Kinne (1999), Wavelength dependence of the optical depth of biomass burning, urban, and desert dust aerosols, *J. Geophys. Res.*, **104**(D24), 31,333–31,349.
- Eck, T. F., et al. (2005), Columnar aerosol optical properties at AERONET sites in central eastern Asia and aerosol transport to the tropical mid-Pacific, *J. Geophys. Res.*, **110**, D06202, doi:10.1029/2004JD005274.
- Exton, H. J., J. Latham, P. M. Park, S. J. Perry, M. H. Smith, and R. R. Allan (1985), The production and dispersal of marine aerosol, *Quart. J. Royal Met. Soc.*, **111**(469), 817–837, doi:10.1002/qj.49711146909.
- Forster, P., et al. (2007), Changes in atmospheric constituents and in radiative forcing, in *Climate Change 2007, the Physical Science Basis: Contribution of Working Group I to the Fourth Assessment Report of the IPCC*, pp. 129–234, Cambridge Univ. Press, Cambridge, U. K.
- Fuentes, E., H. Coe, D. Green, G. de Leeuw, and G. McFiggans (2010), On the impacts of phytoplankton-derived organic matter on the properties of the primary marine aerosol Part 1: Source fluxes, *Atmos. Chem. Phys.*, **10**, 9295–9317, doi:10.5194/acp-10-9295-2010.
- Galanter, M., H. Levy II, and G. R. Carmichael (2000), Impacts of biomass burning on tropospheric CO, NO_x, and O₃, *J. Geophys. Res.*, **105**(D5), 6633–6653.
- Gathman, S. G. (1983), Optical properties of the marine aerosol as predicted by the Navy aerosol model, *Opt. Eng.*, **22**, 57–62.
- Glantz, P., E. D. Nilsson, and W. von Hoyningen-Huene (2009), Estimating a relationship between aerosol optical thickness and surface wind speed over the ocean, *Atmos. Res.*, **92**, 56–68, doi:10.1016/j.atmosres.2008.08.010.
- Gong, S. L. (2003), A parametrization of sea-salt aerosol source function for sub- and super-micron particles, *Global Biogeochem. Cycles*, **17**(4), 1097, doi:10.1029/2003GB002079.
- Grandey, B. S., P. Stier, T. M. Wagner, R. G. Grainger, and K. I. Hodges (2011), The effect of extratropical cyclones on satellite-retrieved aerosol properties over ocean, *Geophys. Res. Lett.*, **38**, L13805, doi:10.1029/2011GL047703.
- Hänel, G. (1976), The properties of atmospheric aerosol particles as functions of the relative humidity at thermodynamic equilibrium with the surrounding moist air, *Adv. Geophys.*, **19**, 73–188, doi:10.1016/S0065-2687(08)60142-9.
- Hansen, J. E., and L. D. Travis (1974), Light scattering in planetary atmospheres, *Space Sci. Rev.*, **16**(4), 527–610, doi:10.1007/BF00168069.
- Hasekamp, O. P., and J. Landgraf (2007), Retrieval of aerosol properties over land surfaces: capabilities of multi-viewing-angle intensity and polarization measurements, *Appl. Opt.*, **46**(16), 3332–3344, doi:10.1364/AO.46.003332.
- Hasekamp, O., P. Litvinov, and A. Butz (2011), Aerosol properties over the ocean from PARASOL multi-angle photopolarimetric measurements, *J. Geophys. Res.*, **116**, D14204, doi:10.1029/2010JD015469.
- Hegg, D. A., J. Livingston, P. V. Hobbs, T. Novakov, and P. Russell (1997), Chemical apportionment of aerosol column optical depth off the mid-Atlantic coast of the United States, *J. Geophys. Res.*, **102**(D21), 25,293–25,303.
- Henderson, B. G., P. Chylek, W. M. Porch, and M. K. Dubey (2006), Satellite remote sensing of aerosols generated by the Island of Nauru, *J. Geophys. Res.*, **111**, D22209, doi:10.1029/2005JD006850.
- Hess, M., P. Koepke, and I. Schult (1998), Optical properties of aerosols and clouds: The software package OPAC, *Bull. Am. Met. Soc.*, **79**(5), 831–944, doi:10.1175/1520-0477(1998)079.
- Hinds, W. C. (1999), *Aerosol Technology: Properties, Behavior, and Measurement of Airborne Particles*, 2nd ed., pp. 75–110, Wiley, New York.

- Holben, B. N., et al. (1998), AERONET: A federated instrument network and data archive for aerosol characterization, *Remote Sens. Environ.*, 66, 1–16, doi:10.1016/S0034-4257(98)00031-5.
- Holben, B. N., et al. (2001), An emerging ground-based aerosol climatology: Aerosol optical depth from AERONET, *J. Geophys. Res.*, 106(D11), 12,067–12,097.
- Holben, B. N., T. F. Eck, I. Slutsker, A. Smirnov, A. Sinyuk, J. Shafer, D. Giles, and O. Dubovik (2006), AERONET's version 2.0 quality assurance criteria, in *Proc. SPIE*, 6408, 64080Q, doi:10.1117/12.706524.
- Hoppel, W. A., J. W. Fitzgerald, G. M. Frick, and R. E. Larson (1990), Aerosol size distributions and optical properties found in the marine boundary layer over the Atlantic Ocean, *J. Geophys. Res.*, 95(D4), 3659–3686.
- Huang, H., G. E. Thomas, and R. G. Grainger (2010), Relationship between wind speed and aerosol optical depth over remote ocean, *Atmos. Chem. Phys.*, 10, 5943–5950, doi:10.5194/acp-10-5943-2010.
- Irshad, R., R. G. Grainger, D. M. Peters, R. A. McPheat, K. M. Smith, and G. E. Thomas (2009), Laboratory measurements of the optical properties of sea salt aerosol, *Atmos. Chem. Phys.*, 9, 221–230, doi:10.5194/acp-9-221-2009.
- Jaeglé, L., P. K. Quinn, T. S. Bates, B. Alexander, and J.-T. Lin (2011), Global distribution of sea salt aerosols: New constraints from in situ and remote sensing observations, *Atmos. Chem. Phys.*, 11, 3137–3157, doi:10.5194/acp-11-3137-2011.
- Kaufman, Y. J., A. Smirnov, B. N. Holben, and O. Dubovik (2001), Base-line maritime aerosol: Methodology to derive the optical thickness and scattering properties, *Geophys. Res. Lett.*, 28(17), 3251–3254.
- Kiliyanpilakkil, V. P., and N. Meskhidze (2011), Deriving the effect of wind speed on clean maritime aerosol optical properties using the A-Train satellites, *Atmos. Chem. Phys.*, 11, 11,401–11,413, doi:10.5194/acpd-11-4599-2011.
- Knobelspiesse, K. D., C. Pietras, G. S. Fargion, M. Wang, R. Frouin, M. A. Miller, A. Subramaniam, and W. M. Balch (2004), Maritime aerosol optical thickness measured by handheld Sun photometers, *Remote Sens. Environ.*, 93(1–2), 87–106, doi:10.1016/j.rse.2004.06.018.
- Kokhanovsky, A. A., et al. (2010), The determination of spectral aerosol optical thickness from satellites: An inter-comparison of algorithms using synthetic backscattered solar light characteristics, *Atmos. Meas. Tech.*, 3, 909–932, doi:10.5194/amt-3-909-2010.
- König-Langlo, G. (2011), *Reference List of Selected Meteorological Datasets from 12 POLARSTERN Cruises With Links to Data*, Alfred Wegener Inst. Polar Mar. Res., Bremerhaven, Germany, doi:10.1594/PANGAEA.771754.
- Kotchenruther, R. A., P. V. Hobbs, and D. A. Hegg (1999), Humidification factors for atmospheric aerosols off the mid-Atlantic coast of the United States, *J. Geophys. Res.*, 104(D2), 2239–2251.
- Lehahn, Y., I. Koren, E. Boss, Y. Ben-Ami, and O. Altartatz (2010), Estimating the maritime component of aerosol optical depth and its dependency on surface wind speed using satellite data, *Atmos. Chem. Phys.*, 10, 6711–6720, doi:10.5194/acp-10-6711-2010.
- Lewis, E. R., and S. E. Schwartz (2004), *Sea Salt Aerosol Production: Mechanisms, Methods, Measurements, and Models*, *Geophys. Monogr. Ser.*, vol. 152, pp. 9–100, 119–182, 256–273, AGU, Washington, D. C.
- Lobert, J. M., and J. M. Harris (2002), Trace gases and air mass origin at Kaashidhoo, Indian Ocean, *J. Geophys. Res.*, 107(D19), 8013, doi:10.1029/2001JD000731.
- Lovett, R. F. (1978), Quantitative measurement of airborne sea-salt in the North Atlantic, *Tellus*, 30, 358–364, doi:10.1111/j.2153-3490.1978.tb00851.x.
- Magi, B. I., P. V. Hobbs, T. W. Kirchstetter, T. Novakov, D. A. Hegg, S. Gao, J. Redemann, and B. Schmid (2005), Aerosol properties and chemical apportionment of aerosol optical depth at locations off the U. S. East Coast in July and August 2001, *J. Atmos. Sci.*, 62(4), 919–933, doi:10.1117/JAS3263.1.
- Mishchenko, M. I., L. D. Travis, R. A. Kahn, and R. A. West (1997), Modeling phase functions for dustlike tropospheric aerosols using a shape mixture of randomly oriented polydisperse spheroids, *J. Geophys. Res.*, 102(D14), 16,831–16,847, doi:10.1029/96JD02110.
- Monahan, E. C., C. W. Fairall, K. L. Davidson, and P. J. Boyle (1983), Observed inter-relations between 10 m winds, ocean whitecaps and marine aerosols, *Quart. J. Royal Met. Soc.*, 109(460), 379–392, doi:10.1002/qj.49710946010.
- Mulcahy, J. P., C. D. O'Dowd, S. G. Jennings, and D. Ceburnis (2008), Significant enhancement of aerosol optical depth in marine air under high wind conditions, *Geophys. Res. Lett.*, 35, L16810, doi:10.1029/2008GL034303.
- Müller, D., A. Ansmann, I. Mattis, M. Tesche, U. Wandinger, D. Althausen, and G. Pisani (2007), Aerosol-type-dependent lidar ratios observed with Raman lidar, *J. Geophys. Res.*, 112, D16202, doi:10.1029/2006JD008292.
- Murray, M. J., M. R. Allen, C. J. Merchant, A. R. Harris, and C. J. Donlon (2000), Direct observations of skin-bulk SST variability, *Geophys. Res. Lett.*, 27(8), 1171–1174.
- O'Dowd, C. D., and G. de Leeuw (2007), Marine aerosol production: A review of the current knowledge, *Philos. Trans. R. Soc. A*, 365, 1753–1774, doi:10.1098/rsta.2007.2043.
- Omar, A. H., D. M. Winker, M. A. Vaughan, Y. Hu, C. A. Trepte, R. A. Ferrare, K.-P. Lee, and C. A. Hostetler (2009), The CALIPSO automated aerosol classification and lidar ratio selection algorithm, *J. Atmos. Oceanic Technol.*, 26, 1994–2014, doi:10.1175/2009JTECHA1231.1.
- O'Neill, N. T., T. F. Eck, A. Smirnov, B. N. Holben, and S. Thulasiraman (2003), Spectral discrimination of coarse and fine mode optical depth, *J. Geophys. Res.*, 108(D17), 4559, doi:10.1029/2002JD002975.
- O'Neill, N. T., T. Eck, A. Smirnov, B. Holben, and S. Thulasiraman (2006), Spectral deconvolution algorithm, *Tech. Rep.*, NASA Goddard Space Flight Cent., Greenbelt, Md.
- Oo, M., and R. Holz (2011), Improving the CALIOP aerosol optical depth using combined MODIS-CALIOP observations and CALIOP integrated attenuated total color ratio, *J. Geophys. Res.*, 116, D14201, doi:10.1029/2010JD014894.
- Pant, V., C. G. Deshpande, and A. A. Kamra (2008), On the aerosol number concentration-wind speed relationship during a severe cyclonic storm over south Indian Ocean, *J. Geophys. Res.*, 113, D02206, doi:10.1029/2006JD008035.
- Pedrés, R., V. Estellés, M. Sicard, J. L. Gómez-Amo, M. P. Utrillas, J. A. Martínez-Lozano, F. Rocadenbosch, C. Pérez, and J. M. B. Recio (2010), Climatology of the aerosol extinction-to-backscatter ratio from Sun-photometric measurements, *IEEE Trans. Geosci. Remote Sens.*, 48(1), 237–249, doi:10.1109/TGRS.2009.2027699.
- Podzimek, J. (1980), Advances in marine aerosol research, *Atmos. Res.*, 14(1), 35–61.
- Reid, J. S., B. Brooks, K. K. Crahan, D. A. Hegg, T. F. Eck, N. O'Neill, G. de Leeuw, E. A. Reid, and K. D. Anderson (2006), Reconciliation of coarse mode sea-salt aerosol particle size measurements and parameterizations at a subtropical ocean receptor site, *J. Geophys. Res.*, 111, D02202, doi:10.1029/2005JD006200.
- Remer, L. A., D. Tanré, and Y. J. Kaufman (2006), Algorithm for remote sensing of tropospheric aerosol from MODIS: Collection 5, *Tech. rep.*, NASA Goddard Space Flight Cent., Greenbelt, Md.
- Reynolds, R. W., T. M. Smith, C. Liu, D. B. Chelton, K. S. Casey, and M. G. Schlax (2006), Daily high-resolution blended analyses for sea surface temperature, *J. Climate*, 20, 5473–5496, doi:10.1175/2007JCLI1824.1.
- Sakerin, S. M., D. M. Kabanov, A. V. Smirnov, and B. N. Holben (2008), Aerosol optical depth of the atmosphere over the ocean in the wavelength range 0.37–4 μm , *Int. J. Remote Sens.*, 29(9), 2519–2547, doi:10.1080/01431160701767492.
- Satheesh, S. K., J. Srinivasan, and K. Krishna Moorthy (2006), Contribution of sea-salt to aerosol optical depth over the Arabian Sea derived from MODIS observations, *Geophys. Res. Lett.*, 33, L03809, doi:10.1029/2005GL024856.
- Sayer, A. M., G. E. Thomas, and R. G. Grainger (2010), A sea surface reflectance model for (A)ATSR, and application to aerosol retrievals, *Atmos. Meas. Tech.*, 3, 813–838, doi:10.5194/amt-3-813-2010.
- Sayer, A. M., N. C. Hsu, C. Bettenhausen, Z. Ahmad, B. N. Holben, A. Smirnov, G. E. Thomas, and J. Zhang (2012), SeaWiFS ocean aerosol retrieval (SOAR): Algorithm, validation, and comparison with other datasets, *J. Geophys. Res.*, 117, D03206, doi:10.1029/2011JD016599.
- Sellegrì, K., C. D. O'Dowd, Y. J. Yoon, S. G. Jennings, and G. de Leeuw (2006), Surfactants and submicron sea spray generation, *J. Geophys. Res.*, 111, D22215, doi:10.1029/2005JD006658.
- Shettle, E. P., and R. W. Fenn (1979), Models for the aerosols of the lower atmosphere and the effects of humidity variations on their optical properties, *Tech. Rep. AFGL-TR-79-0214*, Air Force Geophys. Lab., Hanscom, Mass.
- Silva, A. M., M. L. Bugalho, M. J. Costa, W. von Hoyningen-Huene, T. Schmidt, J. Heintzenberg, and S. Henning (2002), Aerosol optical properties from columnar data during the second Aerosol Characterization Experiment on the south coast of Portugal, *J. Geophys. Res.*, 107(D22), 4642, doi:10.1029/2002JD002196.
- Smirnov, A., Y. Villevalde, N. T. O'Neill, A. Royer, and A. Tarussov (1995), Aerosol optical depth over the oceans: analysis in terms of synoptic air mass types, *J. Geophys. Res.*, 100(D8), 16,639–16,650.
- Smirnov, A., B. N. Holben, T. F. Eck, O. Dubovik, and I. Slutsker (2000a), Cloud-screening and quality control algorithms for the AERONET database, *Remote Sens. Environ.*, 73(3), 337–349.
- Smirnov, A., B. N. Holben, D. Savoie, J. M. Prospero, Y. J. Kaufman, D. Tanre, T. F. Eck, and I. Slutsker (2000b), Relationship between column aerosol optical thickness and in situ ground based dust concentrations over Barbados, *Geophys. Res. Lett.*, 27(11), 1643–1646.

- Smirnov, A., B. N. Holben, O. Dubovik, N. T. O'Neill, L. A. Remer, T. F. Eck, I. Slutsker, and D. Savoie (2000c), Measurement of atmospheric optical properties on U.S. Atlantic coast sites, ships, and Bermuda during TARFOX, *J. Geophys. Res.*, *105*(D8), 9887–9901.
- Smirnov, A., B. N. Holben, Y. J. Kaufman, O. Dubovik, T. F. Eck, I. Slutsker, C. Pietras, and R. H. Halthore (2002), Optical properties of atmospheric aerosol in maritime environments, *J. Atmos. Sci.*, *59*, 501–523.
- Smirnov, A., B. N. Holben, O. Dubovik, R. Frouin, T. F. Eck, and I. Slutsker (2003a), Maritime component in aerosol optical models derived from Aerosol Robotic Network data, *J. Geophys. Res.*, *108*(D1), 4033, doi:10.1029/2002JD002701.
- Smirnov, A., B. N. Holben, T. F. Eck, O. Dubovik, and I. Slutsker (2003b), Effect of wind speed on columnar aerosol optical properties at Midway Island, *J. Geophys. Res.*, *108*(D24), 4802, doi:10.1029/2003JD003879.
- Smirnov, A., B. N. Holben, A. Lyapustin, I. Slutsker, and T. F. Eck (2004), AERONET processing algorithms refinement, paper presented at AERONET Workshop, El Arenosillo, Spain.
- Smirnov, A., et al. (2009), Maritime aerosol network as a component of aerosol robotic network, *J. Geophys. Res.*, *112*, D06204, doi:10.1029/2008JD011257.
- Smirnov, A., et al. (2011), Maritime Aerosol Network as a component of AERONET-first results and comparison with global aerosol models and satellite retrievals, *Atmos. Meas. Tech.*, *4*, 583–597, doi:10.5194/amt-4-583-2011.
- Smirnov, A. V., and K. S. Shifrin (1989), Relationship of optical thickness to humidity of air above the ocean, translated, *Izv. Atmos. Ocean. Phys., Engl. Transl.*, *25*(5), 374–379.
- Wagner, F., and A. M. Silva (2008), Some considerations about Ångström exponent distributions, *Atmos. Chem Phys.*, *8*, 481–489, doi:10.5194/acp-8-481-2008.
- Wallcraft, A. J., A. B. Kara, C. N. Barron, E. J. Metzger, R. L. Pauley, and M. A. Bourassa (2009), Comparisons of monthly mean 10 m wind speeds from satellites and NWP products over the global ocean, *J. Geophys. Res.*, *114*, D16109, doi:10.1029/2008JD011696.
- Zieliński, T., and A. Zieliński (2002), Aerosol extinction and aerosol optical thickness in the atmosphere over the Baltic Sea determined with lidar, *J. Aerosol Sci.*, *33*(6), 907–921, doi:10.1016/S0021-8502(02)00043-5.
- B. N. Holben, N. C. Hsu, and A. Smirnov, NASA Goddard Space Flight Center, Greenbelt, MD 20771, USA.
- A. M. Sayer, Goddard Earth Sciences Technology and Research, Universities Space Research Association, Greenbelt, MD 20771, USA. (andrew.sayer@nasa.gov)